Spatio-temporal Models of Lymphangiogenesis in Wound Healing

Arianna Bianchi, Kevin J. Painter & Jonathan A. Sherratt

Bulletin of Mathematical Biology
A Journal Devoted to Research at the Junction of Computational, Theoretical and Experimental Biology Official Journal of The Society for Mathematical Biology

ISSN 0092-8240

Bull Math Biol
DOI 10.1007/s11538-016-0205-x

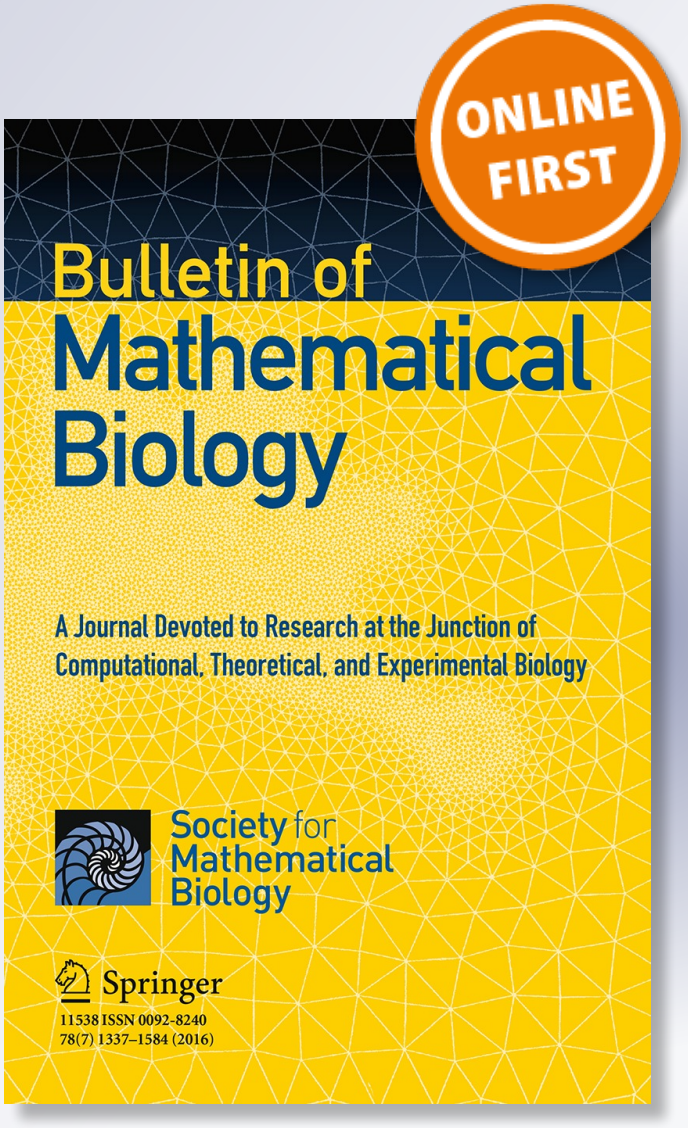

Springer

Bull Math Biol
DOI 10.1007/s11538-016-0205-x

Society for Mathematical Biology

ORIGINAL ARTICLE

Spatio-temporal Models of Lymphangiogenesis in Wound Healing

Arianna Bianchi[1,2] · **Kevin J. Painter**[1] · **Jonathan A. Sherratt**[1]

Received: 15 April 2016 / Accepted: 5 September 2016

Abstract Several studies suggest that one possible cause of impaired wound healing is failed or insufficient lymphangiogenesis, that is the formation of new lymphatic capillaries. Although many mathematical models have been developed to describe the formation of blood capillaries (angiogenesis), very few have been proposed for the regeneration of the lymphatic network. Lymphangiogenesis is a markedly different process from angiogenesis, occurring at different times and in response to different chemical stimuli. Two main hypotheses have been proposed: (1) lymphatic capillaries sprout from existing interrupted ones at the edge of the wound in analogy to the blood angiogenesis case and (2) lymphatic endothelial cells first pool in the wound region following the lymph flow and then, once sufficiently populated, start to form a network. Here, we present two PDE models describing lymphangiogenesis according to these two different hypotheses. Further, we include the effect of advection due to interstitial flow and lymph flow coming from open capillaries. The variables represent different cell densities and growth factor concentrations, and where possible the parameters are estimated from biological data. The models are then solved numerically and the results are compared with the available biological literature.

✉ Arianna Bianchi
arianna.bianchi@ualberta.ca

Kevin J. Painter
K.Painter@hw.ac.uk

Jonathan A. Sherratt
J.A.Sherratt@hw.ac.uk

1 Department of Mathematics and Maxwell Institute for Mathematical Sciences, Heriot-Watt University, Edinburgh EH14 4AS, Scotland, UK

2 Present Address: University of Alberta, 632 Central Academic Building, Edmonton, AB T6G 2G1, Canada

Published online: 26 September 2016

Keywords Wound healing · Lymphangiogenesis · Interstitial flow · Mathematical model

1 Introduction

The lymphatic system first came to the anatomists' attention with Hippocrates' mention of lymph nodes in his fifth century BC work *On Joints* (Withington 1984). Later, the Roman physician Rufus of Ephesus identified the axillary, inguinal and mesenteric nodes and the thymus in the first–second century AD (May 1968). The earliest reference to lymphatic vessels is attributed to the anatomist Herophilus, who lived in Alexandria in the third century BC; he described the lymphatics as "absorptive veins" (Dodson 1924-1925; von Staden 1989). This rudimentary knowledge of the lymphatic system was lost during the Middle Ages, until Gabriele Falloppio re-discovered lymphatic capillaries in the mid-sixteenth century (Castiglioni 1947). Since then, there has been a steady but slow increase in our awareness of the "second" circulatory system of our body (see Ambrose (2006) for an account of immunology's priority disputes in the seventeenth and eighteenth centuries). Major impetus to study the lymphatic system came only in the 1990s, after the discovery of a suitable lymphatic marker that allowed quantifiable observation of lymphatic dynamics (Choi et al. 2012; Oliver and Detmar 2002). Lymphatic research is still a current trend in biomedicine and a source of sensational new discoveries, such as the 2015 finding of lymphatic vessels in the central nervous system (Louveau et al. 2015).

An impetus for studying lymphatic regeneration is provided by recent biological studies that propose lymphangiogenesis as a major target for the treatment of non-healing wounds: functional lymphangiogenesis is nowadays regarded as a crucial factor in wound healing (Cho et al. 2006; Ji 2005; Oliver and Detmar 2002; Witte et al. 2001) and delayed or failed lymphatic regeneration (such as that observed in diabetic patients) constitutes a major cause of impairment to wound healing (Asai et al. 2012; Maruyama et al. 2007; Saaristo et al. 2006).

Interest in lymphatics is therefore not just a mere scientific curiosity: their importance as pressure regulators in tissues and, moreover, as vectors of the immune response has been emphasised in recent decades, particularly in the context of wound healing (Cho et al. 2006; Huggenberger et al. 2011; Ji 2005). The healing of a skin wound is a complex process consisting of different overlapping phases that, if well orchestrated by the organism, lead to the restoration of the skin and vasculature to a healthy, functional condition. Unfortunately, this delicate sequence of events can fail to proceed to full healing in diabetic or aged patients (Asai et al. 2012; Jeffcoate and Harding 2003; Swift et al. 2001); indeed, if the organism response to infection is insufficient, wound healing does not proceed through all normal stages, halting at the inflammation stage and resulting in a chronic wound (Brem and Tomic-Canic 2007; Pierce 2001).

Non-healing wounds constitute a major health problem, seriously affecting the patient's quality of life and accounting for approximately 3 % of all health care expenses in the UK (Drew et al. 2007; Posnett and Franks 2008). Being the main mediators of the immune response, lymphatics seem to significantly contribute to healing (Oliver and Detmar 2002; Witte et al. 2001) and it has been observed that failed lym-

phangiogenesis correlates with impaired wound healing (Asai et al. 2012; Maruyama et al. 2007; Saaristo et al. 2006). However, little is known about the actual mechanisms involved in the lymphangiogenic process, in contrast to the (blood) angiogenic case (Benest et al. 2008; Choi et al. 2012).

Mathematical modelling potentially provides an alternative, powerful tool to back up experimental observations, generate a better understanding of wound healing lymphangiogenesis and identify potential clinical targets. Here, we build upon our ODE model presented in Bianchi et al. (2015) to address the spatial elements of lymphangiogenesis, specifically focussing on modelling two different hypotheses proposed to describe the exact lymphangiogenesis mechanism. In particular, two PDE systems are developed to describe the two hypotheses (named "self-organising" and "sprouting" hypothesis) and their numerical solutions are compared. In addition, more simulations are shown in order to explore the role of two different fluid flows in lymphatic regeneration: the interstitial flow and the lymph flow. Simulations are run for different initial conditions representing shallow and deep wounds.

In the following, Sects. 2.1–2.3 provide an introduction to the biology of wound healing, possible lymphangiogenesis mechanisms and interstitial and lymph flows, respectively. Then, Sect. 3 is devoted to the development of the mathematical models; in particular, a review of existing models is discussed in Sect. 3.1, while the "self-organising hypothesis" is presented in Sect. 3.5 and the "sprouting hypothesis" in Sect. 3.6. In Sect. 3.7, a table with parameter values and sources can be found. Simulations are reported in Sect. 4 and an overall comparison of them is presented in Sect. 4.5. A final discussion is expounded in Sect. 5. Finally, "Appendix" includes a detailed description of how the model parameters were estimated.

2 Biological Background

2.1 Wound Healing

For educational purposes, wound healing is usually presented as a sequence of four different (overlapping) phases, namely:

1. *Haemostasis*: Shortly after injury, a blood clot is formed as a result of the interaction between blood and the extracellular matrix; the clot stops the bleeding and provides a scaffold for cells and chemicals that will consequently contribute to the healing process.
2. *Inflammation*: Substances activated during haemostasis attract *leucocytes*, inflammatory cells which clean the wound from debris and pathogens and secrete chemicals which promote the evolution of the system to the next phase.
3. *Proliferation*: The chemicals released during inflammation enhance the growth and aggregation of the surrounding cells, restoring different tissue functions and elements such as the blood and lymphatic networks; the regeneration of blood and lymphatic vessels is named *(blood) angiogenesis* and *lymphangiogenesis*, respectively. In this phase, the blood clot is slowly substituted by a "temporary dermis" called *granulation tissue*. In parallel with these processes, the rapid proliferation and migration of epidermal cells causes this outer layer of the skin to re-form.

4. *Remodelling*: Finally, the granulation tissue is slowly replaced by normal skin tissue; this stage can take up to 2 years to be completed.

For further details about wound healing, we refer to Singer and Clark (1999) for normal cutaneous wound healing, and to Stadelmann et al. (1998) for an account of chronic wound dynamics.

2.2 Sprouting Versus Self-Organising Lymphangiogenesis

The lymphatic system is a circulatory system responsible for mediating the immune response of the body and maintaining the physiological pressure in tissues by draining excess liquid. It is mainly constituted of vessels and lymph nodes. Lymphatic vessel walls are made of the so-called *lymphatic endothelial cells* (LECs); contrary to the blood case, lymphatic capillaries are very thin and are formed of a single layer of LECs.

To date, little is known about the biological events taking place during lymphangiogenesis and different hypotheses have been proposed by biologists. Although important reviews on the subject such as Norrmen et al. (2011), Tammela and Alitalo (2010) state that lymphangiogenesis "occurs primarily by sprouting from preexisting vessels", in a fashion which resembles the (blood) angiogenic case, recent experiments suggest that this may not be correct, at least not in some specific experimental settings (Benest et al. 2008; Rutkowski et al. 2006). In Benest et al. (2008), it is stated that lymphangiogenesis "can occur both by recruitment of isolated lymphatic islands to a connected network and by filopodial sprouting". Similarly, in Rutkowski et al. (2006) it is reported that in an adult mouse tail wound model, LECs migrate as single cells into the wound space and later connect to each other forming vessel structures (see Fig. 1). According to the authors of Rutkowski et al. (2006), single LEC migration following the lymph/interstitial flow would explain why lymphatic vessel regeneration appears to happen in this direction (from left to right in the figure).

Comparative reviews of lymphangiogenesis and (blood) angiogenesis can be found in Adams and Alitalo (2007), Lohela et al. (2009), Sweat et al. (2012).

2.3 Interstitial Versus Lymph Flow

Interstitial flow is a fluid flow induced by dynamic stresses and pressure gradients through the extracellular matrix. It is generally slower than fluid flow inside vessels, because of the resistance of the extracellular matrix components; nonetheless, interstitial flow has recently been shown to play an important role in many processes, including cell migration. Such effects can be purely mechanical, for example by "pushing" on the cell, or can act indirectly by shifting the distribution of chemicals in the surroundings of the cell. A review of the effects of interstitial flow on cell biology can be found in Rutkowski and Swartz (2007).

In recent years, a number of studies have investigated the role of interstitial flow on lymphangiogenesis, mainly through the formation of concentration gradients of pro-lymphangiogenic factors. In particular, in Boardman and Swartz (2003) the authors propose that interstitial flow, enhanced by the lymph flow resulting from interrupted lymphatic vessels, can direct wound healing lymphangiogenesis by transporting LECs

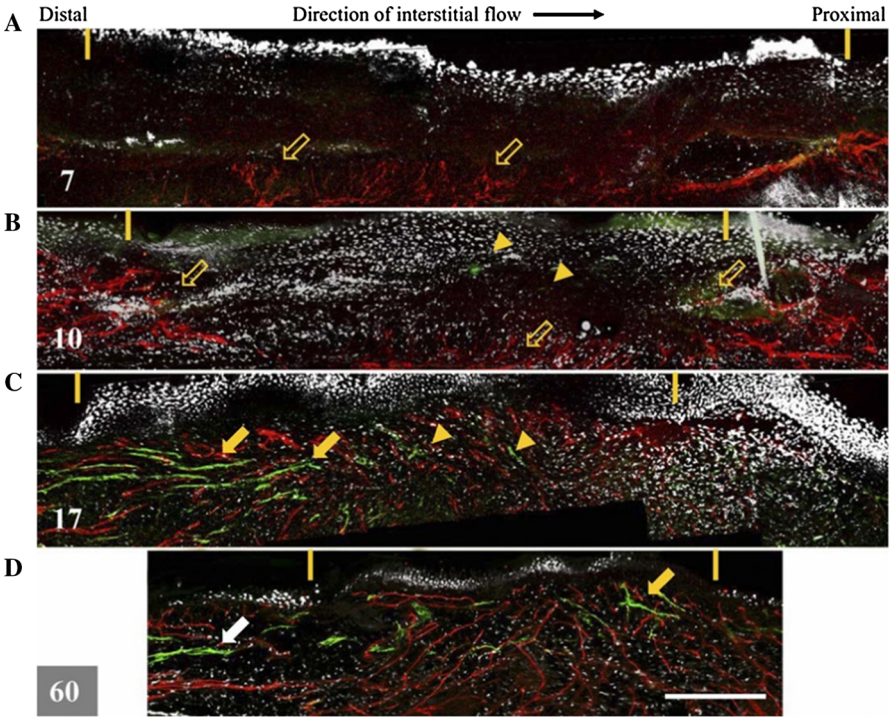

Fig. 1 In the photograph, taken from Rutkowski et al. (2006, Figure 2), one observes blood and lymphatic vessel regeneration in the tail of an adult mouse; lymphangiogenesis appears to occur in the direction of the interstitial flow. The different photographs refer to different times after wounding: **a** Taken at day 7, **b** at day 10, **c** at day 17 and **d** at day 60. The *yellow dashes* mark the regenerating region (note its overall contraction over time); the *red colour* indicates blood vessels, while LEC presence is highlighted by *green colour*. The *open arrows* signal how blood vessels seem to sprout from deeper vessels, while *other arrows* point out LEC organisation at day 17 after a higher LEC density is reached; *arrowheads* indicate single LECs migrating towards the proximal side of the wound. *Scale bar* in **d** = 300μm (Color figure online)

into the wound space and creating gradients in chemicals (such as vascular endothelial growth factor—VEGF) which stimulate LEC growth and chemotaxis.

However, the relative role of interstitial and lymph flow on capillary regeneration has yet to be investigated in depth; therefore, it is not clear which of the two takes on the greatest importance. In fact, although interstitial flow is slower than the flux of the lymph coming from interrupted capillaries, the former persists after wound closure, while the latter is more localised to open capillaries and stops once the lymphatic network has been restored.

3 Mathematical Modelling

3.1 Review of Lymphatic-Related Models

Contrary to the blood angiogenesis case, modelling literature about lymphangiogenesis is relatively immature and sparse, and mostly refers to tumour-induced lymphangio-

genesis (see for instance Friedman and Lolas 2005). To the authors' knowledge, the only models addressing lymphangiogenesis in wound healing are Roose and Fowler (2008), which focuses on the mechanical elements that lend the lymphatic network its characteristic shape (at least in the mouse tail), and our previous work Bianchi et al. (2015), which we are going to extend here. A recent review of mathematical models of vascular network formation is Scianna et al. (2013), where indeed the imbalance between blood angio- and lymphangiogenesis modelling is manifest.

A number of models have been produced by the bioengineering community, describing specific mechanical features of lymphatic physiology; in particular, mechanics of contracting lymph valves have been presented in Galie and Spilker (2009), Heppell et al. (2015), Macdonald et al. (2008), Mendoza and Schmid-Schönbein (2003), Reddy and Patel (1995). A brief review of engineering models proposed in the lymphatic context can be found in Margaris and Black (2012).

Very few attempts have been made to specifically model the effect of flow on capillary regeneration, although one interesting example is Fleury et al. (2006), where the authors use a convection–diffusion model to analyse the effects of flow on matrix-binding protein gradients.

3.2 Model Targets

The model hereby presented aims to investigate the following questions about wound healing lymphangiogenesis:

- which hypothesis (self-organising or sprouting) offers a better explanation for the lymphangiogenesis mechanics?
- what are the relative contributions of interstitial and lymph flow on the lymphangiogenic process?
- how does the initial wounded state impact on lymphatic regeneration?

3.3 Model Variables and Domain

In the following, we propose two similar but distinct PDE models to describe the two different theories advanced by biologists to explain lymphangiogenesis in wound healing (see Sect. 2.2). We will refer to them as the "self-organising" hypothesis (O) and the "sprouting" hypothesis (S).

For both cases, we consider the following basic dynamics: immediately after injury, transforming growth factor-β (TGF-β) is activated and chemotactically attracts macrophages to the wound, which in turn secrete VEGF which induces capillary regeneration acting on either LECs (in the self-organising case) or capillary tips (in the sprouting case). The variables included in the models are summarised in Table 1, where they are reported together with their names and units.

We consider a 1D space variable x that varies between $-\varepsilon$ and $\ell + \varepsilon$; this interval includes the wound space of length ℓ and a portion ε of healthy tissue on its edges [for network structures in two and three dimensions, see Chaplain et al. (2006), Stéphanou et al. (2005), Chaplain and Anderson (1999)]. This kind of domain describes a narrow

Table 1 A summary of the model variables

Variable	Model	Quantity	Units
$T(t,x)$	O, S	Active TGF-β concentration	pg mm^{-3}
$M(t,x)$	O, S	Macrophage density	cells mm^{-3}
$V(t,x)$	O, S	VEGF concentration	pg mm^{-3}
$L(t,x)$	O	Lymphatic endothelial cell density	cells mm^{-3}
$E(t,x)$	S	Lymphatic capillary end (tip) density	cells mm^{-3}
$C(t,x)$	O, S	Lymphatic capillary density	cells mm^{-3}

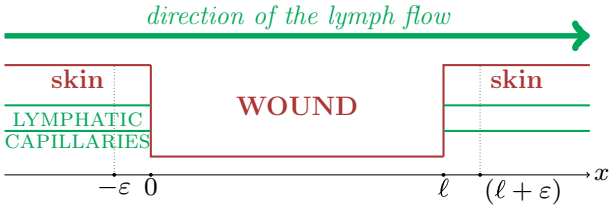

Fig. 2 (Color Figure Online) The model 1D domain: x varies between $-\varepsilon$ and $\ell+\varepsilon$; this interval includes the wound region (which ranges from 0 to ℓ) and part of the healthy tissue containing some intact lymphatic capillaries

cut, where at every point we average chemical and cell densities over the depth of the wound. We take the increasing x-direction to be that of lymph flow (and interstitial flow). A schematic of the model domain is shown in Fig. 2.

3.4 Advection Velocity and Open Capillaries

The models incorporate an advection term for the majority of variables that accounts for the effect of flow on the lymphatic regeneration process. In biological references (such as Boardman and Swartz 2003), it is not clear whether flow is mainly a result of lymph fluid exiting the interrupted capillaries or the "normal" interstitial flow. We hence investigate the relative contribution from these two components by considering an advection term motivated as follows.

In general, interstitial flow does not have a constant direction. However, for simplicity, here we will assume that both lymph and interstitial flow occur in the increasing direction of x (from left to right in Fig. 2); this reflects what is observed in the wound healing experimental setting of Boardman and Swartz (2003), which we take as a reference for model comparison. We assume the interstitial flow to be constant and present across the full tissue, reflecting its persistent nature in healthy tissues. On the other hand, the contribution due to leaking lymphatic capillaries is assumed to depend specifically on the density of open capillaries C_{op} and we assume a linear dependence for simplicity. However, since we do not know the precise contribution of each element to the total advection, we introduce a single "weight" parameter ξ, $0 \leq \xi \leq 1$, which

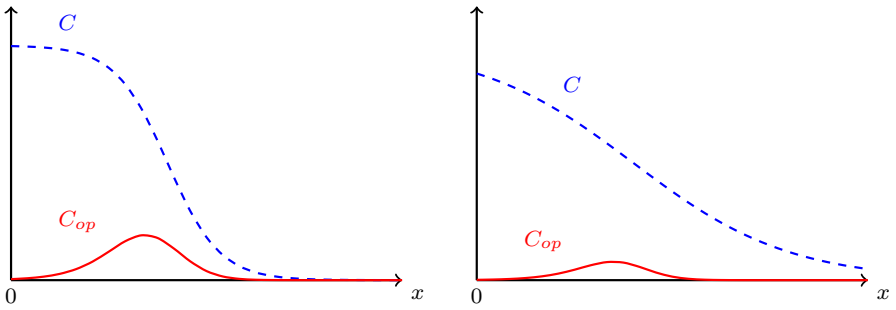

Fig. 3 Plots of C_{op} (*solid red*) for different steepness of C (*dashed blue*) (Color figure online)

can be varied. Specifically, the advection velocities for chemicals and cells, λ^{chem} and λ^{cell}, respectively, will be taken to be of the forms

$$\lambda^{\text{chem}}(C_{\text{op}}) = \xi \cdot (\lambda_1^{\text{chem}} \cdot C_{\text{op}}) + (1-\xi) \cdot \lambda_2^{\text{chem}} \quad \text{and} \tag{1}$$

$$\lambda^{\text{cell}}(C_{\text{op}}) = \xi \cdot (\lambda_1^{\text{cell}} \cdot C_{\text{op}}) + (1-\xi) \cdot \lambda_2^{\text{cell}}, \tag{2}$$

where $0 \leq \xi \leq 1$ and $\lambda_1^{\text{chem}}, \lambda_2^{\text{chem}}, \lambda_1^{\text{cell}}$ and λ_2^{cell} are four parameters to be determined. In "Appendix", we estimate the values of λ_1^{chem} and λ_2^{chem}, while corresponding parameters for cells are assumed to be significantly smaller, since advective cell velocity is likely to be smaller due to the higher environmental friction. A value of $\xi = 0$ corresponds to purely interstitial flow advection, while $\xi = 1$ represents advection due entirely to lymphatic flow.

To quantify the open capillary density, we assume that as the "cut" in capillary density C becomes steeper (and thus $|\partial C/\partial x| \to +\infty$), more capillaries are open and the open capillary density will increase towards its maximum possible value of C, which would correspond to all capillaries being open. We therefore define the open capillary density C_{op} as

$$C_{\text{op}}\left(C, \frac{\partial C}{\partial x}\right) = \frac{|\partial C/\partial x|}{\eta_0 + |\partial C/\partial x|} \cdot C \tag{3}$$

where η_0 is a parameter for whose estimation no relevant experimental data were found. See Fig. 3 for a plot of (3).

3.5 Self-Organising Hypothesis

Under this hypothesis, single LECs migrate into the wound and start to self-organise into capillary structures only after reaching a certain threshold density L^*. This case represents the direct extension of the ODE model developed in Bianchi et al. (2015) and the variable and parameter names have been kept as consistent with Bianchi et al. (2015) as possible.

(Active) TGF-β Equation

The differential equation describing active TGF-β concentration has the following form:

$$\begin{array}{ccccccccc} \text{change in TGF-}\beta \\ \text{concentration} \end{array} = \begin{array}{c} \text{diffusion and} \\ \text{advection} \end{array} + \text{activation} - \text{decay} - \begin{array}{c} \text{internalisation by} \\ \text{macrophages.} \end{array}$$

Of these terms, the following three are assumed to have standard forms:

$$\text{Diffusion: } D_T \frac{\partial^2 T}{\partial x^2} \quad , \quad \text{Decay: } d_1 T \quad , \quad \text{Internalisation: } \gamma_1 T M,$$

and advection will be taken to be $-\partial/\partial x(\lambda^{\text{chem}}(C_{\text{op}}) \cdot T)$, with velocity $\lambda^{\text{chem}}(C_{\text{op}})$ as defined in (1).

Concerning the activation, we consider a constant amount of latent TGF-β in the skin T_L (Taylor 2009; Shi et al. 2011), which is increased by macrophage production at rate r_1 (Khalil et al. 1993). This latent form of TGF-β is activated by macrophages (Taylor 2009; De Crescenzo et al. 2001; Gosiewska et al. 1999; Nunes et al. 1995) and by the enzymes (mainly plasmin) present in the blood clot, which is mainly composed of platelets (Grainger et al. 1995; Hyytiäinen et al. 2004; Khalil et al. 1996) (for a review of TGF-β activation see Taylor 2009). Therefore, we take the following activation term:

$$\underbrace{\left[a_m M + a_p\, p(C)\right]}_{\substack{\text{activation by macro-} \\ \text{-phages \& plasmin}}} \cdot \underbrace{\left[T_L + r_1 M\right]}_{\text{latent TGF-}\beta}.$$

The C-dependent quantity p is an estimate of plasmin presence in the wound, which is proportional to the platelet mass. In fact, although activation of platelet-released TGF-β is still poorly understood, it seems that plasmin, while degrading the blood clot, activates the latent TGF-β contained in the platelets (Grainger et al. 1995). We assume that the plasmin level is proportional to the wound space which is not occupied by capillaries; this is motivated by the fact that capillary presence can be considered as a measure of the healing stage of the wound.[1] When capillary density gets close to its equilibrium (healthy state) value C^{eq} (say 90 % of it), the plasmin-induced TGF-β activation switches to zero. We will thus take

$$p(C) = \begin{cases} -\frac{\psi}{9/10 \cdot C^{\text{eq}}} C + \psi & \text{if } C \leq (C^{\text{eq}} \cdot 9/10) \\ 0 & \text{if } C \geq (C^{\text{eq}} \cdot 9/10). \end{cases} \tag{4}$$

[1] An alternative approach would be to consider fibroblasts instead of capillaries here, but the introduction of a new variable and consequently a new equation does not seem to be worthwhile, since capillary presence is a good indication of the healing state of the wound.

Macrophage Equation

The following scheme will be considered for macrophage dynamics:

change in macrophage density	=	random movement and advection	+	chemotaxis by TGF-β	+	constant source	+	influx from open capillaries
	−	removal and differentiation	−	crowding effect.				

Macrophages are assumed to move randomly with diffusion coefficient μ_M, while their advection will be modelled by the term $-\frac{\partial}{\partial x}\left(\lambda^{\text{cell}}(C_{\text{op}}) \cdot M\right)$, with $\lambda^{\text{cell}}(C_{\text{op}})$ as discussed in Sect. 3.4.

For the chemotaxis term, we first point out that only a fraction α of the monocytes that are chemoattracted by TGF-β differentiate into (inflammatory) macrophages (Mantovani et al. 2004; Wahl et al. 1987). Therefore, the term describing macrophage chemotaxis up TGF-β gradients will have the form

$$-\alpha\chi_1 \frac{\partial}{\partial x}\left(\frac{M}{1+\omega M} \cdot \frac{\partial T/\partial x}{1+\eta_1 |\partial T/\partial x|}\right)$$

where the macrophage velocity $\frac{1}{1+\omega M} \cdot \frac{\partial T/\partial x}{1+\eta_1|\partial T/\partial x|}$ decreases as cell density increases [as in Velázquez (2004a), Velázquez (2004b)] and is bounded as $|\partial T/\partial x| \to \infty$. The presence of a constant source s_M (from the bottom of the wound) is justified by the observation that the macrophage equilibrium in unwounded skin is nonzero (Weber-Matthiesen and Sterry 1990).

The introduction of an influx term is motivated by the fact that macrophages are "pumped out" from interrupted capillaries (Boardman and Swartz 2003; Rutkowski et al. 2006) and into the wound. We consider the following form for the influx term:

$$\varphi_1\left(C_{\text{op}}, \frac{\partial C}{\partial x}\right) = C_{\text{op}} \cdot \zeta_1\left(\frac{\partial C}{\partial x}\right), \tag{5}$$

where C_{op} was introduced in (3) and ζ_1 is defined as

$$\zeta_1\left(\frac{\partial C}{\partial x}\right) = \begin{cases} \phi_1 \text{ if } \partial C/\partial x < 0 \\ 0 \text{ otherwise .} \end{cases} \tag{6}$$

In (6) ϕ_1 is a parameter estimated in "Appendix". The Heaviside form of ζ_1 is due to the influx only occurring from the open lymphatic capillaries on the side of the wound from which lymph fluid flows (see Fig. 2).

The removal term includes (inflammatory) macrophage death, differentiation into repair macrophages and reintroduction into the vascular system, with the latter being proportional to the capillary density. Thus, we take the removal term to be $(d_2+\rho C)M$. We also include a crowding effect through the term $-\frac{M+L+C}{k_1} \cdot M$.

VEGF Equation

For VEGF we assume the following dynamics:

change in VEGF concentration	=	diffusion and advection	+	constant source	+	production by macrophages
	−	decay	−	internalisation by LECs.		

VEGF diffusion is modelled via the standard term $D_V \frac{\partial^2 V}{\partial x^2}$ and advection by $-\frac{\partial}{\partial x}\left(\lambda^{\text{chem}}(C_{\text{op}}) \cdot V\right)$ where $\lambda^{\text{chem}}(C_{\text{op}})$ is the expression defined in (1). The constant source is called s_V, while the production term will be $r_3 M$ and the decay $d_3 V$. Internalisation is assumed to be linearly dependent on LEC density, and the corresponding term will consequently be $\gamma_2 V L$.

LEC Equation

The equation describing the presence of LECs in the wound consists of the following terms:

change in LEC density	=	random movement and advection	+	chemotaxis by VEGF	+	growth, upregulated by VEGF and downregulated by TGF-β
	+	influx from open capillaries	−	crowding effect	−	transdifferentiation into capillaries.

Again, random cell movement is modelled via a diffusion term $\mu_L {}^{\partial^2 L}/_{\partial x^2}$ and the advection is taken to be $-\frac{\partial}{\partial x}\left(\lambda^{\text{cell}}(C) \cdot L\right)$.

LECs are chemoattracted by VEGF (Bernatchez et al. 1999; Tammela and Alitalo 2010), and the chemotaxis term is assumed to be of a similar form to that used to describe macrophage chemotaxis:

$$-\chi_2 \frac{\partial}{\partial x}\left(\frac{L}{1+\omega L} \cdot \frac{{}^{\partial V}/_{\partial x}}{1+\eta_2 \left|{}^{\partial V}/_{\partial x}\right|}\right).$$

LEC growth is upregulated by VEGF (Bernatchez et al. 1999; Whitehurst et al. 2006; Zachary and Gliki 2001) and downregulated by TGF-β (Müller et al. 1987; Sutton et al. 1991):

$$\left(c_1 + \frac{V}{c_2 + c_3 V}\right)\left(\frac{1}{1+c_4 T}\right) L.$$

LECs are "pumped out" from the interrupted capillaries in a similar manner to macrophages, but also result (with less intensity) from interrupted capillaries downstream of the lymph flow. The influx term this time takes the form:

$$\varphi_2\left(C_{\text{op}}, \frac{\partial C}{\partial x}\right) = C_{\text{op}} \cdot \zeta_2\left(\frac{\partial C}{\partial x}\right) \tag{7}$$

where C_{op} is the density of open capillaries as in (3) and ζ_2 is defined as

$$\zeta_2\left(\frac{\partial C}{\partial x}\right) = \begin{cases} \phi_2^+ \text{ if } \partial C/\partial x < 0 \\ \phi_2^- \text{ if } \partial C/\partial x > 0, \end{cases} \tag{8}$$

where $\phi_2^+ > \phi_2^-$.

LECs cannot grow excessively due to crowding, which is taken into account via the term $-\frac{(M+L+C)}{k_2} \cdot L$. When LECs have *locally* sufficiently populated the wound [i.e. when their density exceeds a threshold L^* (Boardman and Swartz 2003; Rutkowski et al. 2006)], they are assumed to self-organise into capillaries at a rate which is increased by the presence of VEGF (Podgrabinska et al. 2002):

$$\sigma(L, C) \cdot (\delta_1 + \delta_2 V)L$$

where

$$\sigma(L, C) = \begin{cases} 1 \text{ if } L + C \geq L^* \\ 0 \text{ if } L + C < L^*. \end{cases} \tag{9}$$

Lymphatic Capillary Equation

After LECs have occupied enough of the wound space, they coalesce into a capillary network; also, they undergo remodelling, which we model via a logistic term. Thus, the C-equation will be

$$\underbrace{\sigma(L, C) \cdot (\delta_1 + \delta_2 V)L}_{\text{source}} + \underbrace{c_5\left(1 - \frac{C}{k_3}\right)C}_{\text{remodelling}}.$$

Observe that no advection term is present here, since capillary structures are collections of cells attached to each other and thus are more resistant to the interstitial flows.

Full System: "Self-Organising" Hypothesis

The full system of equations in the "self-organising" hypothesis is therefore given by

$$\begin{aligned} \frac{\partial T}{\partial t} &= D_T \frac{\partial^2 T}{\partial x^2} - \frac{\partial}{\partial x}\left(\lambda^{\text{chem}}(C_{\text{op}}) \cdot T\right) + \left[a_m M + a_p p(C)\right] \cdot [T_L + r_1 M] \\ &\quad - d_1 T - \gamma_1 T M, \end{aligned} \tag{10}$$

$$\begin{aligned} \frac{\partial M}{\partial t} &= \mu_M \frac{\partial^2 M}{\partial x^2} - \frac{\partial}{\partial x}\left(\lambda^{\text{cell}}(C_{\text{op}}) \cdot M + \alpha\chi_1 \frac{M}{1 + \omega M} \cdot \frac{\partial T/\partial x}{1 + \eta_1 |\partial T/\partial x|}\right) \\ &\quad + s_M + \varphi_1\left(C_{\text{op}}, \frac{\partial C}{\partial x}\right) - (d_2 + \rho C)M - \frac{M + L + C}{k_1} M, \end{aligned} \tag{11}$$

$$\frac{\partial V}{\partial t} = D_V \frac{\partial^2 V}{\partial x^2} - \frac{\partial}{\partial x}\left(\lambda^{\text{chem}}(C_{\text{op}}) \cdot V\right) + s_V + r_3 M - d_3 V - \gamma_2 V L, \tag{12}$$

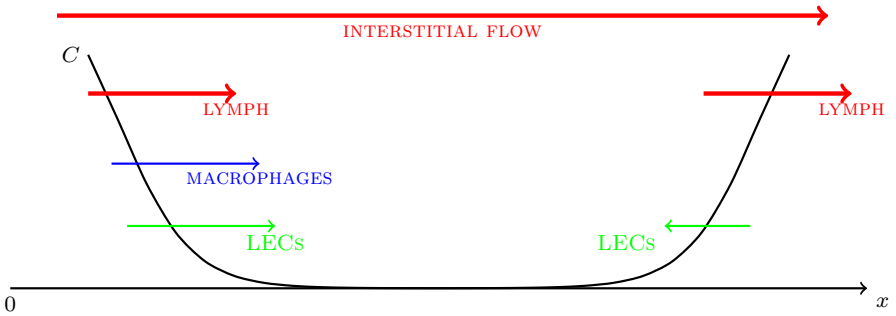

Fig. 4 (Color Figure Online) A summary of the fluxes included in the model: capillaries; fluid fluxes; macrophage influx; and LEC influx (only in O)

$$\frac{\partial L}{\partial t} = \mu_L \frac{\partial^2 L}{\partial x^2} - \frac{\partial}{\partial x}\left(\lambda^{\text{cell}}(C_{\text{op}}) \cdot L + \chi_2 \frac{L}{1+\omega L} \cdot \frac{\partial V/\partial x}{1+\eta_2 |\partial V/\partial x|}\right) + \left(c_1 + \frac{V}{c_2 + c_3 V}\right)\left(\frac{1}{1+c_4 T}\right) L + \varphi_2\left(C_{\text{op}}, \frac{\partial C}{\partial x}\right) - \frac{M+L+C}{k_2} L - \sigma(L, C) \cdot (\delta_1 + \delta_2 V) L, \tag{13}$$

$$\frac{\partial C}{\partial t} = \sigma(L, C) \cdot (\delta_1 + \delta_2 V) L + c_5 \left(1 - \frac{C}{k_3}\right) C, \tag{14}$$

where λ^{chem} is defined in (1), λ^{cell} in (2), p in (4), φ_1 in (5), φ_2 in (7) and σ in (9). Parameters, initial and boundary conditions, are discussed in Sects. 3.7 and 3.8, respectively. See Fig. 4 for a summary of the fluxes included in the model.

3.6 Sprouting Hypothesis

Here, instead of LECs we consider capillary tip density E. Capillary tips are attached to the vessel ends, and therefore, contrary to LECs, are not subject to advection. As we will see, the introduction of this variable is necessary in order to model directed capillary growth in response to a gradient. Examples of mathematical models of blood angiogenesis (in wound healing and in tumours) which include the capillary tip variable can be found in Byrne and Chaplain (1995), Byrne et al. (2000), Flegg et al. (2012), Flegg et al. (2015), Levine et al. (2001), Mantzaris et al. (2004) and Schugart et al. (2008).

TGF-β, macrophage and VEGF equations are the same as in the self-organising case, except that in both the crowding term for M and the V internalisation term there is E instead of L.

Lymphatic Capillary Ends (Tips) Equation

Capillary ends (or tips) are assumed to sprout from interrupted lymphatic capillaries, the density of which (C_{op}) was defined in (3). Tip growth is enhanced by VEGF and inhibited by TGF-β, and this is reflected by the following term, similar to the one used

for LECs in the self-organising case:

$$\left(c_1 + \frac{V}{c_2 + c_3 V}\right)\left(\frac{1}{1 + c_4 T}\right) C_{\text{op}}.$$

Importantly, capillary ends move in the direction of the (positive) gradient of VEGF with an upper-bounded velocity, modelled by the term

$$-\chi_2 \frac{\partial}{\partial x}\left(E \cdot \frac{\partial V/\partial x}{1 + \eta_2 \left|\partial V/\partial x\right|}\right).$$

Finally, we assume that capillary tip death is due predominantly to overcrowding and thus we include the removal term $-\frac{(M+E+C)}{k_2} \cdot E$.

Lymphatic Capillary Equation

New capillaries are formed continuously from the interrupted ones in the direction defined by their tips. This is modelled here according to the "snail trail" concept which was introduced in Edelstein (1982) for fungal colonies and which has been widely used in models of (blood) angiogenesis (Flegg et al. 2012): newly formed capillaries are laid after the sprouting tips, which therefore leave a sort of "track" behind.

Capillaries also undergo remodelling. Therefore, their dynamics are captured by the terms:

$$\underbrace{\chi_2 \left| E \cdot \frac{\partial V/\partial x}{1 + \eta_2 \left|\partial V/\partial x\right|} \right|}_{\text{sprouting}} + \underbrace{c_5 \left(1 - \frac{C}{k_3}\right) C}_{\text{remodelling}}.$$

Full System: "Sprouting" Hypothesis

Thus, the full system for the "sprouting" hypothesis is

$$\begin{aligned}
\frac{\partial T}{\partial t} &= D_T \frac{\partial^2 T}{\partial x^2} - \frac{\partial}{\partial x}\left(\lambda^{\text{chem}}(C_{\text{op}}) \cdot T\right) + \left[a_m M + a_p p(C)\right] \cdot \left[T_L + r_1 M\right] \\
&\quad - d_1 T - \gamma_1 T M, \qquad (15) \\
\frac{\partial M}{\partial t} &= \mu_M \frac{\partial^2 M}{\partial x^2} - \frac{\partial}{\partial x}\left(\lambda^{\text{cell}}(C_{\text{op}}) \cdot M + \alpha \chi_1 \frac{M}{1 + \omega M} \cdot \frac{\partial T/\partial x}{1 + \eta_1 \left|\partial T/\partial x\right|}\right) \\
&\quad + s_M + \varphi_1\left(C_{\text{op}}, \frac{\partial C}{\partial x}\right) - (d_2 + \rho C) M - \frac{M + E + C}{k_1} M, \qquad (16) \\
\frac{\partial V}{\partial t} &= D_V \frac{\partial^2 V}{\partial x^2} - \frac{\partial}{\partial x}\left(\lambda^{\text{chem}}(C_{\text{op}}) \cdot V\right) + s_V + r_3 M - d_3 V - \gamma_2 V E, \qquad (17)
\end{aligned}$$

$$\frac{\partial E}{\partial t} = \left(c_1 + \frac{V}{c_2 + c_3 V}\right)\left(\frac{1}{1 + c_4 T}\right) C_{\text{op}} - \chi_2 \frac{\partial}{\partial x}\left(E \cdot \frac{\partial V/\partial x}{1 + \eta_2 |\partial V/\partial x|}\right) - \frac{M + E + C}{k_2} E, \tag{18}$$

$$\frac{\partial C}{\partial t} = \chi_2 \left| E \cdot \frac{\partial V/\partial x}{1 + \eta_2 |\partial V/\partial x|} \right| + c_5 \left(1 - \frac{C}{k_3}\right) C, \tag{19}$$

where λ^{chem} is defined in (1), λ^{cell} in (2), p in (4), φ_1 in (5) and C_{op} in (3) (see Fig. 4 for a summary of the fluxes of the model).

We recall that the main differences between the two systems consist of the fourth and fifth equation. Equation (13) in the self-organising system describes LEC dynamics, while Eq. (18) represents the evolution of capillary tips. Equations (14) and (19) portray the actual capillary formation under the self-organising and sprouting hypothesis, respectively.

3.7 Parameters

All the model parameters are reported in Table 2. Many of the parameters were estimated previously in Bianchi et al. (2015), and we refer to this source for details of their estimation. For the other parameters listed in Table 2, the details of their estimation can be found in "Appendix".

3.8 Initial and Boundary Conditions

Initial Conditions

As initial time $t = 0$, we take the moment of wounding, when little chemical or cell populations are assumed to have entered in the wound space. Specifically, we assume that at $t = 0$ there are no LECs (for model O) or capillary tips (for S), while other variables can be present near the edges (recall our domain includes portions of healthy skin surrounding the wound). We will then take the following initial conditions:

$$\nu(0, x) = a_\nu \cdot \left[1 - \frac{\tanh(bx) + \tanh(b(-x + \ell))}{2}\right], \tag{20}$$

$$L(0, x) = E(0, x) = 0, \tag{21}$$

where $\nu \in \{T, M, V, C\}$. For each variable ν the value of a_ν is chosen to be such that $\nu(0, -\varepsilon) = \nu(0, \ell + \varepsilon)$ is equal to the boundary conditions discussed in the following. Concerning b, we will vary its value to see how the "sharpness" of the initial condition will affect lymphangiogenesis. For higher values of b, the initial conditions become more step-like and we can interpret this as a deep wound with sharp edges: in this case, there would be (almost) no capillaries in the centre of the wound. On the other hand, assigning smaller values of b would correspond to a shallower initial wound, such that when averaging over the wound depth a certain number of capillaries still

Table 2 List of parameters appearing in the model equations; those referred to Bianchi et al. (2015) for details are the same as in the ODE model therein presented, while estimation of the newly introduced ones is discussed in "Appendix"

Parameter	Value	Units	Source	Details
D_T	2.76	$\text{mm}^2\text{day}^{-1}$	Lee et al. (2014); Murphy et al. (2012)	"Appendix"
η_0	10^4	cells mm^{-4}	No data found	"Appendix"
λ_1^{chem}	1.35×10^{-2}	mmday^{-1}	Fischer et al. (1996), Fischer et al. (1997)	"Appendix"
λ_2^{chem}	8.64×10^2	mmday^{-1}	Rutkowski and Swartz (2007)	"Appendix"
a_p	2.9×10^{-2}	$\text{mm}^3\text{pg}^{-1}\text{day}^{-1}$	De Crescenzo et al. (2001)	Bianchi et al. (2015)
ψ	10^5	pg mm^{-3}	No data found	"Appendix"
a_m	0.45	$\text{mm}^3\text{cells}^{-1}\text{day}^{-1}$	Gosiewska et al. (1999), Nunes et al. (1995)	Bianchi et al. (2015)
T_L	18	pg mm^{-3}	(Oi et al. (2004))	Bianchi et al. (2015)
r_1	3×10^{-5}	$\text{pg cells}^{-1}\text{day}^{-1}$	Khalil et al. (1993)	Bianchi et al. (2015)
d_1	5×10^2	day^{-1}	Kaminska et al. (2005)	Bianchi et al. (2015)
γ_1	4.2×10^{-3}	$\text{mm}^3\text{cells}^{-1}\text{day}^{-1}$	(Yang et al. (1999))	"Appendix"
μ_M	0.12	$\text{mm}^2\text{day}^{-1}$	Farrell et al. (1990)	"Appendix"
λ_1^{cell}	1.35×10^{-3}	mmday^{-1}	Estimated $\approx 0.1 \times \lambda_1^{\text{chem}}$	"Appendix"
λ_2^{cell}	86.4	mmday^{-1}	Estimated $\approx 0.1 \times \lambda_2^{\text{chem}}$	"Appendix"
α	0.5	1	Waugh and Sherratt (2006)	Bianchi et al. (2015)
χ_1	4×10^{-2}	$\text{mm}^5\text{pg}^{-1}\text{day}^{-1}$	Li Jeon et al. (2002)	"Appendix"
ω	1.67×10^{-6}	$\text{mm}^3\text{cells}^{-1}$	Estimated $\approx 1/k_1^{old}$	"Appendix"
η_1	100	$\text{mm}^9\text{pg}^{-1}$	No data found	"Appendix"
s_M	8.6×10^2	$\text{cells mm}^{-3}\text{day}^{-1}$	(Weber-Matthiesen and Sterry (1990))	"Appendix"
ϕ_1	2.05×10^3	day^{-1}	Cao et al. (2005), Fischer et al. (1996)	"Appendix"
β	5×10^{-3}	1	Greenwood (1973)	Bianchi et al. (2015)
r_2	1.22	day^{-1}	Zhuang and Wogan (1997)	Bianchi et al. (2015)
d_2	0.2	day^{-1}	Cobbold and Sherratt (2000)	Bianchi et al. (2015)
ρ	10^{-5}	$\text{day}^{-1}\text{cells}^{-1}$	Rutkowski et al. (2006)	Bianchi et al. (2015)
k_1	10^5	$\text{mm}^3\text{cells}^{-1}$	Zhuang and Wogan (1997)	"Appendix"
D_V	2.4	$\text{mm}^2\text{day}^{-1}$	Miura and Tanaka (2009)	"Appendix"
s_V	1.94	cells day^{-1}	(Hormbrey et al. (2003), Papaioannou et al. (2009))	Bianchi et al. (2015)

Table 2 continued

Parameter	Value	Units	Source	Details
r_3	1.9×10^{-3}	pg cells^{-1}day^{-1}	(Kiriakidis et al. (2003), Sheikh et al. (2000))	Bianchi et al. (2015)
d_3	11	day^{-1}	Kleinheinz et al. (2010)	Bianchi et al. (2015)
γ_2	1.4×10^{-3}	mm^{3}cells^{-1}day^{-1}	Gabhann (2004)	Bianchi et al. (2015)
μ_L	0.1	mm^{2}day^{-1}	Estimated $\approx \mu_M$	"Appendix"
c_1	0.42	day^{-1}	Nguyen et al. (2007)	Bianchi et al. (2015)
c_2	42	day	Whitehurst et al. (2006)	Bianchi et al. (2015)
c_3	4.1	pg day mm^{-3}	Whitehurst et al. (2006)	Bianchi et al. (2015)
c_4	0.24	mm^{3}pg^{-1}	Müller et al. (1987)	Bianchi et al. (2015)
χ_2	0.173	mm^{5}pg^{-1}day^{-1}	Barkefors et al. (2008)	"Appendix"
η_2	1	mm^{9}pg^{-1}	No data found	"Appendix"
ϕ_2^+	10^2	day^{-1}	No data found	"Appendix"
ϕ_2^-	1	day^{-1}	Estimated to be 1 % of ϕ_2^+	"Appendix"
k_2	4.71×10^5	cells day mm^{-3}	Nguyen et al. (2007)	Bianchi et al. (2015)
L^*	10^4	cells mm^{-3}	Rutkowski et al. (2006)	Bianchi et al. (2015)
δ_1	5×10^{-2}	day^{-1}	No data found	Bianchi et al. (2015)
δ_2	10^{-3}	mm^{3}pg^{-1}day^{-1}	No data found	Bianchi et al. (2015)
c_5	0.42	day^{-1}	Estimated = c_1	"Appendix"
k_3	1.2×10^4	mm^{3}cells^{-1}	Estimated $\approx C^{\text{eq}}$	"Appendix"

Each parameter is supplied with its estimated value, units and source used (when possible) to assess it. References in brackets mean that although the parameter was not *directly* estimated from a data set, its calculated value was compared with the biological literature; the caption "no data found" signifies that no suitable data were found to estimate the parameter. Note that a_m here corresponds to a_M in Bianchi et al. (2015) and γ_2 here to γ in Bianchi et al. (2015). k_1^{old} denotes the parameter k_1 in Bianchi et al. (2015), where it is the macrophage-carrying capacity. The parameter d_4 appears in the boundary conditions for L

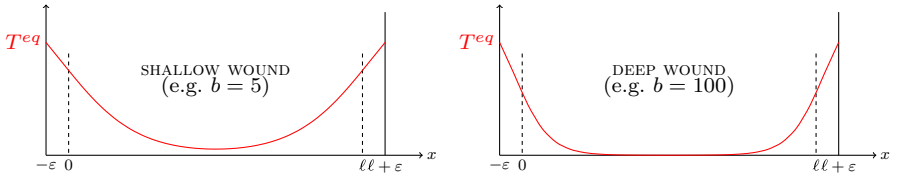

Fig. 5 (Color Figure Online) Initial condition $T(0, x) = a_T \cdot \{1 - [\tanh(b(x-\varepsilon))) + \tanh(b(-x+\ell-\varepsilon))]/2\}$ for different values of b. T^{eq} denotes the T-equilibrium level in non-wounded skin

remain. As an example, the plot of (20) for $\nu = T$ is shown in Fig. 5 for different values of b.

Boundary Conditions

First of all, note that boundary conditions are not needed for C. We consider Dirichlet boundary conditions for all other variables except L, for which we assume Robin

boundary conditions. The choice of Dirichlet boundary conditions is dictated by the fact that at the boundary the tissue is in a non-wounded state, and we expect variables to remain close to their normal, equilibrium value there. For L, we apply instead the following reasoning.

For LECs, we assume that once they pass the domain edge they move randomly and die at a constant rate d_4; in fact, it seems unrealistic to assume that they will just vanish once reaching the domain edge. Therefore, we will follow common practice for representation of habitat boundaries in ecological modelling (Ludwig et al. 1979): we set a different evolution equation for L inside and outside the domain. In the interior (i.e. for $-\varepsilon < x < \ell + \varepsilon$), the dynamics of L will be described by the Eq. (13); in the exterior (i.e. for $x < -\varepsilon$ and $x > \ell + \varepsilon$) instead we assume that LECs move randomly and die (or transdifferentiate) with (high) constant rate d_4. This gives the equation

$$\frac{\partial L}{\partial t} = \mu_L \frac{\partial^2 L}{\partial x^2} - d_4 L \tag{22}$$

outside the wound, whose solution at equilibrium is given by

$$L_o(x) = A_o \exp\left(\sqrt{\frac{d_4}{\mu_L}}x\right) + B_o \exp\left(-\sqrt{\frac{d_4}{\mu_L}}x\right) \tag{23}$$

where A_o and B_o are constants. Note that, since we want solutions to be bounded in order to be biologically meaningful, we will take $B_o = 0$ for $x < -\varepsilon$ and $A_o = 0$ for $x > \ell + \varepsilon$. Since at the boundaries the outside and the inside solutions should have the same value and the same flux, we have that

$$\text{at } x = -\varepsilon: \quad L = A_o \ \text{ and } \ \frac{\partial L}{\partial x} = A_o\sqrt{\frac{d_4}{\mu_L}} \quad \Rightarrow \ \frac{\partial L}{\partial x}(t, -\varepsilon) = \sqrt{\frac{d_4}{\mu_L}}L(t, 0)$$

$$\text{at } x = \ell + \varepsilon: \quad L = B_o \exp\left(-\sqrt{\frac{d_4}{\mu_L}}\ell\right) \ \text{ and } \ \frac{\partial L}{\partial x} = -B_o\sqrt{\frac{d_4}{\mu_L}} \exp\left(-\sqrt{\frac{d_4}{\mu_L}}\ell\right)$$

$$\Rightarrow \ \frac{\partial L}{\partial x}(t, \ell + \varepsilon) = -\sqrt{\frac{d_4}{\mu_L}}L(t, \ell)$$

which give the boundary conditions for L.

Summarising, the boundary conditions are

$$v(t, -\varepsilon) = v(t, \ell + \varepsilon) = v^{\text{eq}}\ , \ E(t, -\varepsilon) = E(t, \ell + \varepsilon) = 0, \tag{24}$$

$$\frac{\partial L}{\partial x} - \sqrt{\frac{d_4}{\mu_L}}L = 0 \quad \text{at } x = -\varepsilon\ , \ \frac{\partial L}{\partial x} + \sqrt{\frac{d_4}{\mu_L}}L = 0 \quad \text{at } x = \ell + \varepsilon \tag{25}$$

with $v \in \{T, M, V, C\}$ and where v^{eq} denotes the equilibrium value in the unwounded skin for each variable.

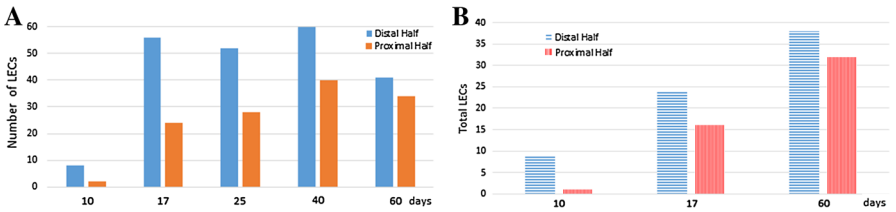

Fig. 6 (Color Figure Online) Quantification of LEC presence and distribution in the regenerating region of a mouse tail wound. Here, the total numbers of LECs in the distal and proximal halves of the wound at different days post-wounding are reported after data from **a** Rutkowski et al. (2006, Figure 2) and **b** Goldman et al. (2007, Figure 1)

4 Numerical Solutions

To simulate the two systems (10)–(14) and (15)–(19), a specific code was written which applies the Crank–Nicolson method for the diffusion terms and a first-order upwind scheme for the chemotactic terms.

This section is structured as following: first, in Sect. 4.1, we present the data sets which will be used as reference points in estimating the "goodness" of the simulations; then, in Sect. 4.2 we present a sample simulation of both the whole O and S models; in Sect. 4.3 we explore how changes in b (initial condition steepness) and ξ (interstitial/lymph flow balance) affect lymphatic regeneration; in Sect. 4.4, we address the two extreme cases where there is no advection at all and where the two advection terms sum up (*additive advection*); finally, in Sect. 4.5 we summarise all the observations concerning the different behaviour of O and S systems.

4.1 Data for Comparison

We will compare our model simulations with experimental data reported in Fig. 6. These experimental observations show that the overall levels of LECs (both free and in a capillary structure) increase steadily after wounding and that while at day 10 the vast majority are in the distal half (i.e. upstream the lymph flow) by 60 days they are almost evenly distributed over the two sides.

Hence, from experimental data:

- lymphatics should have reached a density close to C^{eq} at day 60;
- LEC migration and/or lymphatic capillary formation should happen predominantly in the direction of the lymph/interstitial flow.

4.2 A First Simulation of O and S

We start by presenting simulations of the self-organising and sprouting cases (Figs. 7, 8, respectively) with $\xi = 0.5$ (representing that interstitial and lymph flow are equally weighted in the overall advection term) and a very smooth initial condition, with $b = 5$ [see (20)].

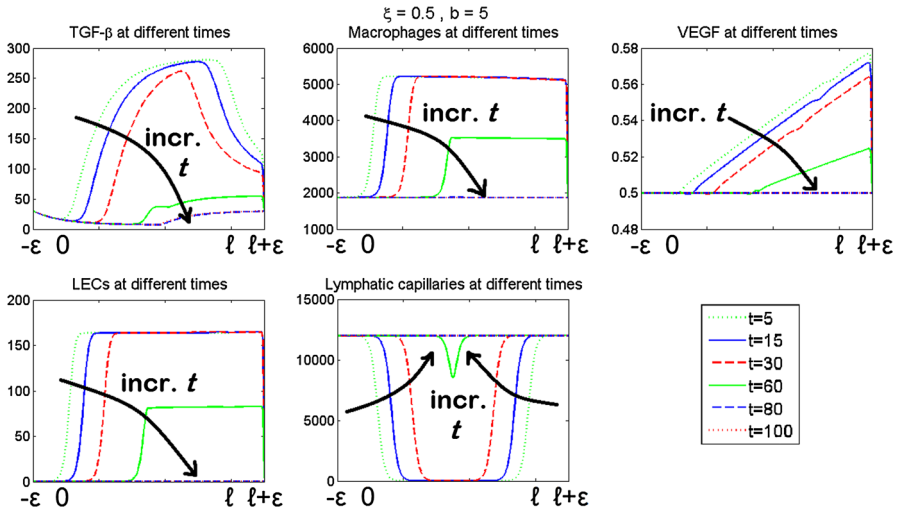

Fig. 7 (Color Figure Online) Simulation of equations (10)–(14) (self-organising case) with parameters from Table 2 and initial condition as defined in Sect. 3.8, with $b = 5$; $\xi = 0.5$. *Arrows* mark the direction of increasing t in the simulations

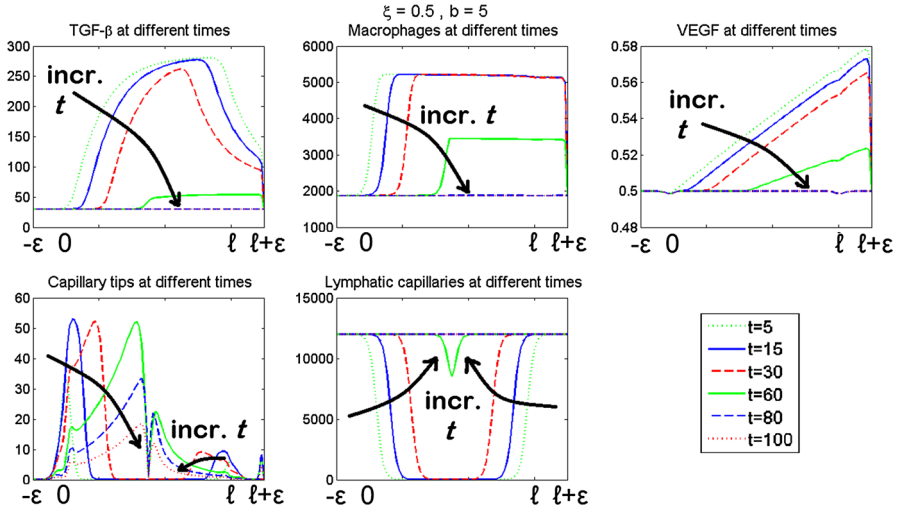

Fig. 8 (Color Figure Online) Simulation of equations (15)–(19) (sprouting case) with parameters from Table 2 and initial condition as defined in Sect. 3.8, with $b = 5$; $\xi = 0.5$. *Arrows* mark the direction of increasing t in the simulations

For these values of ξ and b, both systems predict lymphatic regeneration to be almost symmetric and a nearly complete network is restored by around day 60 (see Figs. 7, 8). Biologically, this represents the situation in which a relatively shallow wound leaves more capillaries in the domain after wounding, so that regeneration occurs mainly from remodelling of the preexisting network. We note, however, that the distribution of the other variables is highly asymmetric. This will lead to a non-

symmetric lymphatic regeneration when parameters are changed so that the chemical concentrations contribute more prominently to the lymphangiogenesis process. One unexpected feature emerging from Figs.7 and 8 is that macrophage, VEGF and LEC levels are higher than equilibrium in the healthy tissue on the right-hand side of the wound, downstream the lymph flow. While some overspill is likely to be observed, particularly macrophage density appears to be too high to be realistic. In Sect. 4.3, we will present results suggesting that the value $\xi = 0.5$ used in Figs. 7 and 8 is inappropriately low; the high downstream densities are a consequence of this. However, an additional possible explanation might be that more processes are involved in bringing cell and chemical levels back to normal in the healthy skin surrounding a wound; macrophages are likely to be "re-absorbed" in the blood and lymphatic vasculature, where their number is balanced by factors not included in the model. However, the simulations shown in Figs. 7 and 8 do predict that eventually all the variables' amounts go back to equilibrium as healing proceeds.

4.3 Varying b and ξ

"Visual" observations In order to clearly visualise the changes in dynamics when the parameters b and ξ are varied, we report the approximate solution profiles of the lymphatic capillary density at different times for different combinations of these two parameters; such simulations are reported in Tables 3 and 4 for the self-organising and the sprouting case, respectively.

In the self-organising case, we observe that varying ξ between 0 and 0.75 does not significantly affect the model output for capillary regeneration; on the other hand, the initial conditions play a crucial role, since for a shallow wound ($b = 5$) the lymphatic

Table 3 Plots of capillary density at different times for different values of b and ξ in the self-organising case [Eqs. (10)–(14)]; arrows mark the direction of increasing t in the simulations

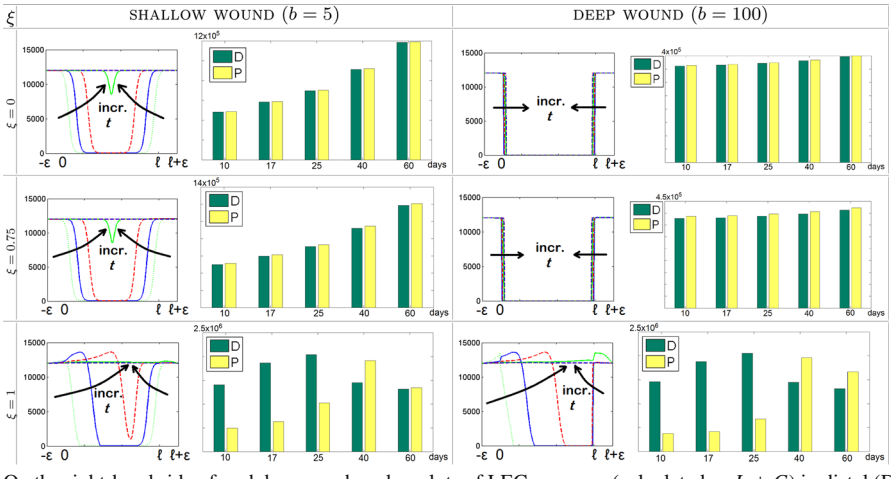

On the right-hand side of each box, we show bar plots of LEC presence (calculated as $L + C$) in distal (D) and proximal (P) half of the wound at days 10, 15, 25, 40 and 60 for different values of b and ξ

Table 4 Plots of capillary density at different times for different values of b and ξ in the sprouting case [Eqs. (15)–(19)]; arrows mark the direction of increasing t in the simulations

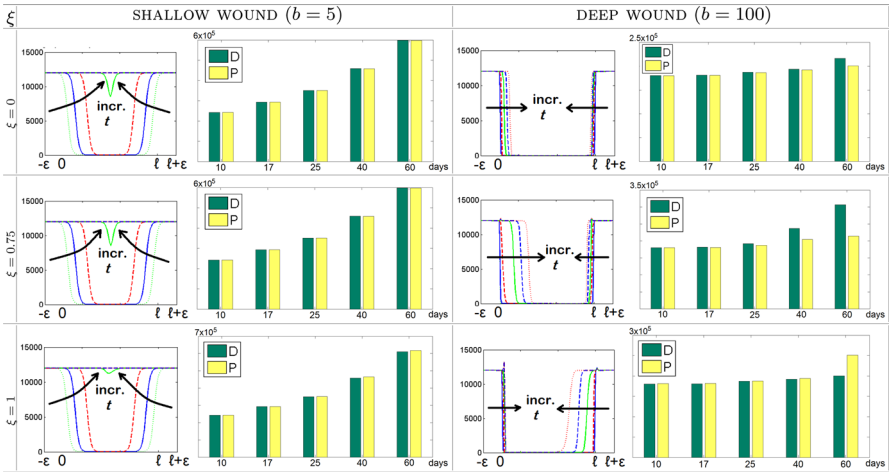

On the right-hand side of each box, we show bar plots of LEC presence (calculated as $E + C$) in distal (D) and proximal (P) half of the wound at days 10, 15, 25, 40 and 60 for different values of b and ξ

network is almost completely restored by day 60, while almost no healing is observed in the deep wound ($b = 100$) scenario. In addition, lymphangiogenesis happens in a fairly symmetric fashion. However, things appear to be quite different for $\xi = 1$: in this case, both shallow and deep wounds exhibit a left-to-right lymphangiogenic process, which is completed by day 60. Note that while lymphangiogenesis occurs *exclusively* from left to right in the deep wound scenario, in the shallow wound some lymphatic regeneration is also visible from the right-hand side of the wound; this confirms our first observation that in a shallow wound logistic remodelling plays a more prominent role than in the deep wound setting. These results suggest that the self-organising hypothesis is supported by the assumption that lymph flow, rather than interstitial flow, is the main contributor to advection in the wound space.

For the sprouting case, things are almost identical to the self-organising case for $0 \leq \xi \leq 0.75$ and $b = 5$ (shallow wound scenario). However, varying ξ in this range seems to proportionally increase the left-to-right regeneration speed in the deep wound case ($b = 100$), although it is still unable to account for complete regeneration at day 60. In addition, for $\xi = 1$, while symmetric (although faster) healing is still visible for $b = 5$, a capillary front advancing from right to left emerges in the deep wound scenario, though again this is not fast enough to restore the network by day 60. This apparent "switch" of behaviour can be explained as follows. $\xi = 1$ corresponds to an advection component due exclusively to lymph flow coming from interrupted capillaries; hence, where $C_{\text{op}} = 0$ both cells and chemicals tend to accumulate on one side of the wound. In the self-organising case, however, LECs display random movement and allow the capillary front to move. In the sprouting scenario, on the other hand, capillary tips are not subject to either diffusion or advection; therefore, the front of open capillaries tends to be stuck on the left-hand side of the wound and

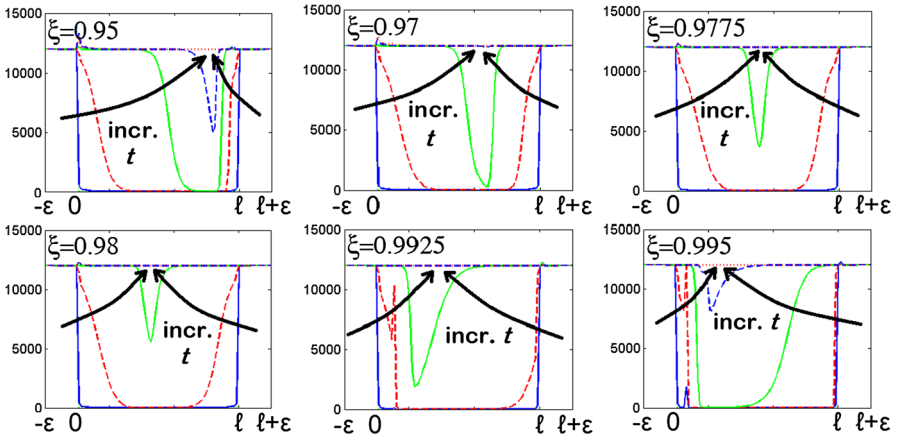

Fig. 9 (Color Figure Online) Sprouting case: capillary density dynamics at different times for different values of ξ in the range 0.75–1 ($\xi = 0.95, 0.97, 0.9775, 0.98, 0.9925, 0.995$—*from left to right*, *top to bottom*, respectively), with $b = 100$ (deep wound scenario). *Arrows* mark the direction of increasing t in the simulations

chemotaxis tends to happen from right to left. Thus, there is not such an obvious correlation between the value of ξ and the validity of the sprouting hypothesis, in contrast to what we have seen above for the self-organising case. In the sprouting case, a very precise balance of lymph and interstitial flow is required to give a left-to-right lymphangiogenesis which is "fast enough," that is one which completes by day 60.

To further investigate the "switch" of behaviour (from left-to-right to vice versa) observed in Table 4 for $b = 100$, we run some extra simulations of this case for $0.75 < \xi < 1$. Results are reported in Fig. 9 (note that no significant difference is observed for $0.75 < \xi < 0.95$; thus, we report extra simulations only for values of ξ starting from 0.95).

The simulations in Fig. 9 suggest that sprouting lymphangiogenesis switches from being left-to-right to being right-to-left as ξ increases from 0 to 1, passing through symmetrical healing at around $\xi = 0.9775$.

Therefore, the most "realistic" value for ξ seems to be $\xi_O \approx 1$ for the self-organising case and $\xi_S \approx 0.97$ for the sprouting case. For these values,

the self-organising case predicts total healing by day 60 (in accordance with the data discussed in Sect. 4.1), while the sprouting case is a bit delayed in this respect. However, all the variables go back to their equilibrium levels in the latter case, while TGF-β, macrophages and VEGF stay at a high concentration in the right-hand side of the wound in the self-organising scenario, which is not what we would expect to happen in reality (simulations not shown).

Quantitative observations In order to make these observations more quantitative and compare them directly with the data sets presented in Sect. 4.1; in each case (i.e. both hypotheses and both combinations of ξ and b values), we calculate a parameter π_{60} to quantify the percentage of healing/lymphatic regeneration at day 60. We also count

Table 5 Values of π_{60} [defined in (26)] for different values of ξ and b in the self-organising (O) and sprouting (S) cases

	Shallow wound ($b = 5$)				
ξ	0	0.25	0.5	0.75	1
O	97.2 %	97.2 %	97.2 %	97.3 %	101.7 %
S	97.1 %	97.1 %	97.1 %	97.1 %	99.2 %
	Deep wound ($b = 100$)				
ξ	0	0.25	0.5	0.75	1
O	5.1 %	5.1 %	5.2 %	5.2 %	104.1 %
S	6.6 %	8.3 %	10.5 %	17.5 %	10.6 %

how many LECs are present in the left (distal) and right (proximal) half of the domain at days 10, 17, 25, 40 and 60; in this way, we can directly compare the model output with the empirical data reported in Fig. 6.

To define the quantity π_{60}, we consider one slice of the wound space, as depicted in Fig. 2; we then consider the ratio between the space occupied by the lymphatic capillaries at day 60 and the original wound space. Thus, we consider

$$\pi_{60} = 100 \cdot \frac{S_{C,60} - S_{IC}}{S_{\text{wound}}}, \tag{26}$$

where $S_{C,60}$ is calculated as the area under the C-curve at $t = 60$ (approximated as a polygon using the numerical results shown above) and $S_{\text{wound}} = C^{\text{eq}} \cdot (\ell + 2\varepsilon) - S_{IC}$; S_{IC} denotes the area subtended by the capillary initial profile curve defined in (20), with $\nu = C$. In this way, we estimate the portion of the *real* initial wound (i.e. excluding the preexisting capillary density) occupied by capillaries at day 60. The values of π_{60} for the various cases considered above are reported in Table 5.

From Table 5, we can see clearly how at day 60 the lymphatic vasculature will be restored to a level of 97 % or more for any value of ξ in the shallow wound simulations in both the self-organising and sprouting cases. For a deeper wound, however, the lymphatic capillary population is restored only up to about 5 % in the self-organising case and up to about 17 % in the sprouting case for $\xi \leq 0.75$; also, while the parameter π_{60} has more or less the same value for all these ξ's in the self-organising case, we observe an increase in π_{60} for increasing ξ in the sprouting scenario (from 6 to 17 %). For $\xi = 1$, though, the healing predictions are quite different: in the self-organising case, lymphatic capillary density slightly exceeds 100 % healing, while the sprouting case exhibits a capillary regeneration that covers only 10 % of the original wound.

To compare the model predictions with the data reported in Fig. 6, we plot the number of LECs (considered as $L + C$ and $E + C$ in the self-organising and sprouting case respectively) in the left (distal) and right (proximal) half of the domain at days 10, 17, 25, 40 and 60. Such numbers are reported as bars in Tables 3 and 4 (right-hand side of each box), which correspond exactly to the cases plotted in Tables 3 and 4 as simulations.

Comparing and contrasting the bar plots reported in Tables 3 and 4 (right-hand side of each box) with the data sets in Fig. 6, we see that the row corresponding to

$\xi = 1$ is by far the best match for the self-organising case (the other values of ξ giving almost no difference between the distal and proximal LEC density in any day after wounding). For the sprouting case, it is natural to make a different distinction: lymphatic regeneration is always predicted to happen symmetrically in a shallow wound; in a deep wound, a slight distal-biased LEC density is observed appearing at days 40 and 60 for $\xi \leq 0.75$, while for $\xi = 1$ the LEC density in the proximal half of the wound overtakes that in the distal half by day 60.

These observations confirm our first intuition: the self-organising case requires a value of ξ close to one in order to observe a realistically fast left-to-right lymphangiogenesis, while the sprouting hypothesis needs a value of ξ between 0.75 and 1 to produce similarly good results. This difference could be explained by the different mechanisms regulating lymphangiogenesis in each case. In the self-organising hypothesis, capillaries form from LEC self-aggregation and disposition in capillary structures once these are (locally) sufficiently abundant; a constant ever-going interstitial flow slows this down because it prevents local LEC accumulation. In contrast, lymph flow occurs only nearby interrupted capillary fronts, which move on as LECs coalesce into vessels. In the sprouting case, by contrast, the total absence of interstitial flow is a problem because neither capillary tips nor well-formed capillaries are subject to either random movement or lymph flow from interrupted capillaries; hence, interstitial flow is the only movement-inducing force, aside from chemical gradients. Moreover, in order to observe a chemical concentration peak on the right-hand side of the wound (which, by chemotaxis, would induce a left-to-right migration of capillary tips), a good balance is required between an everywhere-present interstitial flow and a locally active lymph flow.

4.4 No Advection and Additive Advection Cases

We now consider two final cases: that of no advection at all and that with *additive* advection (that is, where the advection velocity is as in (1) and (2), but without the coefficients involving the parameter ξ).

Simulations of the no advection case are shown in Table 6 for both the self-organising and sprouting models.

Note that, in the self-organising case, dynamics in the absence of advection resemble those reported in Table 3 for $\xi = 1$, although here capillary regeneration is a bit slower. Here, the driving force behind left-to-right lymphangiogenesis is the influx of macrophages (which produce VEGF) and LECs (which form capillaries) from the left side of the interrupted capillaries. (Recall the influx term from the right edge is zero for macrophages and very small for LECs.)

In the sprouting case, too, capillary density evolution reflects that previously observed for $\xi = 1$ (see Table 4). However, contrary to the self-organising case, here dynamics are significantly faster in the absence of advection. The reason behind this may lie in macrophages accumulating on the left side on the wound: consequently so does VEGF, which then drives the capillary sprouting from the right towards the peak on the left. Observe that here there are no LECs coming from the open capillaries on the left, so the regeneration is solely directed by gradients (capillary tips move towards increasing gradients of VEGF).

Table 6 Simulation of the self-organising (O) and sprouting (S) systems with parameters from Table 2 and initial condition as defined in Sect. 3.8 where the advection terms are switched to zero

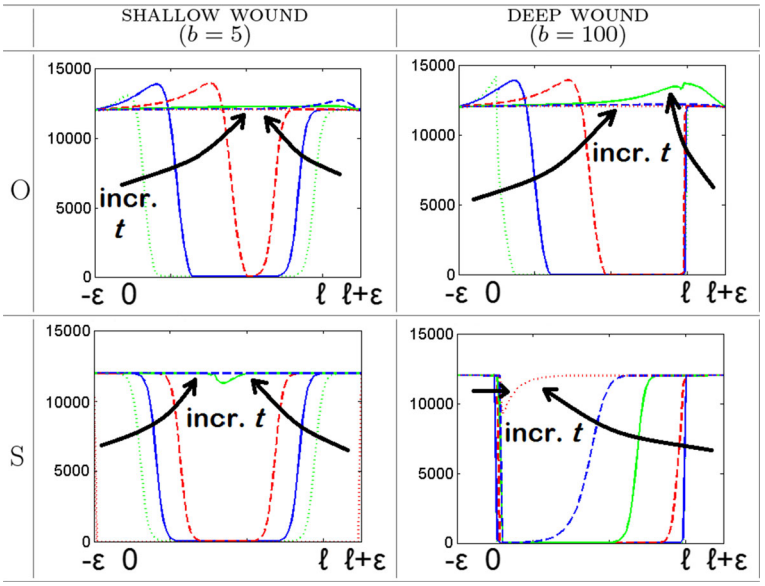

Arrows mark the direction of increasing t in the simulations

These results suggest two conclusions regarding advection:

1. advection contributes to the *speed* of the lymphatic regeneration, speeding up the process in the self-organising case and slowing it down under the sprouting hypothesis;
2. advection is of greater importance in the sprouting case, where it actually determines the direction (left-to-right or vice versa) in which healing occurs.

In other words, while the self-organising hypothesis seems to be able to explain left-to-right lymphangiogenesis on its own (thanks to the free LECs influx, primarily from the left side), the sprouting system needs some kind of force pushing VEGF towards the right of the domain so as to form a gradient driving capillary sprouts from the distal to the proximal end of the wound.

Finally, we investigate what happens when the advection velocities for chemicals and cells are replaced, respectively, by

$$\lambda^{\text{chem}}(C_{\text{op}}) = (\lambda_1^{\text{chem}} \cdot C_{\text{op}}) + \lambda_2^{\text{chem}} \quad \text{and} \tag{27}$$

$$\lambda^{\text{cell}}(C_{\text{op}}) = (\lambda_1^{\text{cell}} \cdot C_{\text{op}}) + \lambda_2^{\text{cell}}; \tag{28}$$

we call this the *additive advection* case. This time lymphangiogenesis, while not appearing overly affected in the shallow wound case, is heavily slowed down in the deep wound scenario (simulation not shown). This reflects the fact that, when lymphatic regeneration is driven mainly by chemical gradients, a sufficiently strong

advection force has a negative effect in healing because it does not allow chemicals and cells to accumulate, thereby producing sufficiently steep gradients.

4.5 Overall Comparison of O and S

Here, the overall similarities and differences between the self-organising and sprouting hypotheses are summarised:

- In shallow wounds lymphangiogenesis appears to be dominated by logistic growth/remodelling and occurs symmetrically from both sides of the wound. In this case, there is little difference between the two hypotheses in terms of the dynamics of wound healing lymphangiogenesis.
- Steeper initial conditions (as in a deep wound) lead to slower capillary regeneration; this is reasonable, since smaller/shallower wounds are expected to heal faster (Vowden 2011; Zimny et al. 2002) (see also Monstrey et al. (2008) for burn depth). In the deep wound case, we also observe a marked difference in behaviour between the two hypotheses: the self-organising case exhibits a very slow progression for values of ξ not close to 1, with the empirically observed speed occurring for $\xi = 1$; by contrast, the sprouting hypothesis predicts lymphangiogenesis to take place from left to right at a speed that increases with ξ up to $\xi \approx 0.9775$, when it becomes symmetric; for larger ξ healing switches to a right-to-left process, at decreasing speed as ξ approaches 1. This variety of behaviour highlights how important the "balance" between interstitial and lymph flow is in the advection terms (1) and (2).

5 Discussion

The results presented in this paper provide new insights in the understanding of lymphangiogenesis mechanisms. Wound healing lymphangiogenesis is increasingly considered a fundamental aspect of the regeneration process, but there is still no consensus in the scientific community about how this phenomenon takes place. In particular, two main hypotheses have been advanced to describe the lymphangiogenesis process: the self-organising hypothesis (Benest et al. 2008; Rutkowski et al. 2006) and the sprouting hypothesis (Norrmen et al. 2011; Tammela and Alitalo 2010). Here, we propose two different PDE systems to describe the two sets of assumptions. The present work shows how the problem of determining the exact lymphatic regeneration mechanism is intertwined with another open question in cellular biology: is interstitial flow a determining factor in cell migration? (Rutkowski and Swartz 2007) In this paper, we explore the more general case of the effects of advection due to the combination of interstitial flow and lymph flow coming from the interrupted capillaries. In addition, we also consider how different initial conditions, corresponding to shallow and deep wounds, affect the healing process.

The numerical simulations of the two systems we propose as describers for the self-organising and sprouting hypotheses suggest that the observation of left-to-right lymphangiogenesis does not justify *per se* the self-organising hypothesis: our

sprouting-hypothesis system can also reproduce this phenomenon, although for a very precise balance of lymph and interstitial flow. Therefore, a reliable value of ξ is needed in order to choose between the two hypotheses. Other discriminating factors are that:

- capillary density in the sprouting case never significantly exceeds its normal value C^{eq}, while overcoming this value is predicted in the self-organising case;
- in the self-organising case, there is an excess of TGF-β, macrophages and VEGF persisting downstream of the lymph flow after capillaries have reached their healthy equilibrium level.

Biologically, it is not clear which is the main contributor to advection between interstitial flow and lymph flow coming from the interrupted capillaries; the models that we have presented suggest the latter is more relevant and that the value of ξ is above 0.75 in both modelled hypotheses. Moreover, our simulations hint at an inhibiting action of interstitial flow on lymphangiogenesis: strong interstitial flow here seems to significantly slow down capillary regeneration. This may be attributed to the fact that a ubiquitous advection force prevents chemical gradients from forming on the "correct" side of the wound.

Finally, initial conditions (that is, the type of wound, shallow or deep) strongly affect the speed and shape of the regeneration process: deeper wounds require more time to heal, and lymphangiogenesis will occur more markedly in the direction of the lymph flow in this case.

Our results emphasise the importance of advection in tissue regeneration; this concept could be of particular importance in describing the emerging concept of *autologous chemotaxis*, that is the phenomenon whereby a cell can receive directional cues while at the same time being the source of such cues (see Rutkowski and Swartz 2007, Shields et al. 2007).

Further developments of the model could include the blood vasculature, so as to allow a direct comparison between the regenerations of the two vessel structures. The model could also be adapted to investigate differences in lymphatic regeneration in a diabetic scenario, as in Bianchi et al. (2015). It would also be interesting to investigate the similarities and the differences between wound healing lymphangiogenesis and tumour lymphangiogenesis: tumour cells are known to release lymphangiogenic factors and the tumour mass alters tissue pressure and interstitial flow, which could in turn promote pathological lymphangiogenesis in cancer (Cao 2005; Christiansen and Detmar 2011; Lunt et al. 2008; Rofstad et al. 2014; Simonsen et al. 2012).

A definitive answer to the question of whether the self-organising or sprouting hypothesis better describes lymphangiogenesis will require a more informed evaluation of the relative contribution of interstitial and lymph flow to advection in the wound space, and more detailed spatio-temporal measures of capillary density and chemical concentrations: do we observe a "bump" exceeding normal capillary density along the capillary healing front? Do TGF-β, macrophages and VEGF persist at a high-level downstream of the lymph flow after lymphatic regeneration is complete?

Acknowledgments A.B. was funded in part by a Maxwell Institute Scholarship from Heriot-Watt University. K.J.P. acknowledges partial support from BBSRC Grant BB/J015940/1.

Appendix: Parameter Estimation

Sizes, Weights, Equilibria and Velocities

Domain Size

We consider a full-thickness wound of length $\ell = 5$ mm, inspired by Zheng et al. (2007). For the surrounding skin, we consider a (small) variable width ε. Thus, we have a domain of length 5 mm $+ 2\varepsilon$. In all the simulations reported in the present paper, $\varepsilon = 1$; the nature of the observations does not change if a different value of ε is chosen (simulations not shown).

TGF-β Molecular Weight and Equilibrium T^{eq}

We take TGF-β molecular weight to be approximately 25 kDa (Boulton et al. 1997; Wakefield et al. 1988, active/mature isoform). The equilibrium value of active TGF-β is about 30 pg/mm^3 (Yang et al. 1999, Figure 2).

Macrophage Volume and Equilibrium M^{eq}

A human alveolar macrophage has a volume $V_{M\Phi}$ of approximately $5000\mu\mathrm{m}^3 = 5 \times 10^{-6}\mathrm{mm}^3$ (Krombach et al. 1997). The macrophage steady state can be estimated from Weber-Matthiesen and Sterry (1990, Figure 1), which plots typical macrophage density in the skin. This shows that there is an average of about 15 macrophages per $0.1\mathrm{mm}^2$ field. Assuming a visual depth of 80 μm, the macrophage density becomes 15 cells/$(0.1\mathrm{mm}^2 \times 0.08\mathrm{mm}) = 1875$ cells/mm^3.

VEGF Molecular Weight and Equilibrium V^{eq}

VEGF molecular weight is taken to be 38 kDa (Kaur and Yung 2012; Yang et al. 2009, VEGF-165). The VEGF equilibrium concentration is estimated to be 0.5 pg/mm^3 from Hormbrey et al. (2003, Figure 1) and Papaioannou et al. (2009, Figure 2).

Normal Capillary Density C^{eq}

In Rutkowski et al. (2006), we find that "it was not until *day 60*, when functional and continuous lymphatic capillaries appeared normal" and "at *day 60* the regenerated region had a complete lymphatic vasculature, the morphology of which appeared similar to that of native vessels". Hence, we assume that a capillary network that can be considered "final" appears at day 60, and we take C^{eq} to be the number of LECs present at this time. In Rutkowski et al. (2006, Figure 2E), we see that at that time there are about 80 cells. This value corresponds to a 12 μm thin section. In addition, from Rutkowski et al. (2006, Figure 2D) we can calculate the observed wound area, which is about 5.6×10^5 μm^2. In this way, we get a volume of 0.0067 mm^3 with 80 cells, which corresponds to $C^{\mathrm{eq}} = 1.2 \times 10^4$ cells/mm^3.

Maximum Capillary Density $C_{\max}$

First of all, we want to convert 1 capillary section into a cell number. For this purpose, we assume EC cross-sectional dimensions to be those reported in Haas and Duling (1997), namely $10\,\mu$m $\times$ $100\,\mu$m. We then assume that LECs lie "longitudinally" along the capillaries, and therefore, only the short dimension contributes to cover or "wrap" the circumference of the capillary. Considering a capillary diameter of 55 μm as in Fischer et al. (1996), we have that each lymphatic capillary section is made of approximately 20 LECs (taking into account some overlapping). Then, from van der Berg et al. (2003) we know that EC thickness is approximately 0.5 μm. Thus, a capillary section is a circle of about $55 + 2 \times 0.5\,\mu$m diameter, corresponding, as described above, to 20 cells.

If we imagine stacking 1 mm^3 with capillaries of this size, we see that we can pile on 1 mm/56 μm $\approx$ 18 layers of capillaries. Then, considering an EC length of 100 μm as in Haas and Duling (1997), we have that 1 mm^3 fits at most a number of capillaries equivalent to the following amount of ECs:

$$20 \text{ cells } \times 18 \times 18 \times \frac{1 \text{ mm}}{100\,\mu\text{m}} \approx 6.4 \times 10^4 \text{ cells } = C_{\max} .$$

Lymph Velocity

Fischer et al. (1996) suggests that the high lymph flow value (0.51mm/s) is due to high pressure following die injection. This suggests that a lower value (9.7 microns/s) might be considered as typical, in agreement with Fischer et al. (1997). In both papers, the normal lymph velocity seems to be around 10 microns/s.

We thus assume lymph velocity to be $v_{\text{lymph}} = 10$ micron/s $= 864$ mm/day (from Fischer et al. 1996, 1997).

Interstitial Flow Velocity

First of all, we note that in Rutkowski and Swartz (2007) interstitial flow in the skin is calculated to be around 10 microns/s. [Note that Helm et al. (2005) is relevant for this aspect of our modelling, although it is less important for the estimation of parameters; in this reference, the synergy between interstitial flow and VEGF gradient is discussed.] Therefore, we will consider the interstitial flow to be also $v_{IF} = 10$ microns/s $= 864$ mm/day (from Rutkowski and Swartz 2007).

Re-calculation of s_M and k_1

s_M here is calculated in the same way as in Bianchi et al. (2015), but using our amended model equations presented here. For k_1, we point out that in Bianchi et al. (2015) this parameter was appearing in the logistic part of the M-equation: $dM/dt = r_2 M - r_2/k_1 \cdot M^2$. In the PDE systems, we do not include such terms because only a minor fraction of macrophages undergo mitosis (Greenwood 1973). However,

death due to overcrowding is present in both models; comparing these terms, we see that our "new" k_1 corresponds to the "old" k_1/r_2.

Diffusion Coefficients

VEGF Diffusion Coefficient D_V

In Miura and Tanaka (2009), the authors observe that "in general, the diffusion coefficient of protein molecules in liquid is of the order of $10^6\ \mu\text{m}^2/\text{h} = 24\ \text{mm}^2/\text{day}$. This intuitively means that a molecule moves 10 μm/s. To generate a gradient over the order of 100 μm, the timescale of protein decay should be around 10 s. In this specific case, the protein decay time is about 1–10 h. Therefore, the observed diffusion coefficient is too large and we need some mechanism to slow down the diffusion" (where "this specific case" means that of VEGF).

In Miura and Tanaka (2009) the VEGF diffusion coefficient is estimated in three different ways: by a theoretical model ($0.24\ \text{mm}^2/\text{day}$), and by two different empirical techniques ($24\ \text{mm}^2/\text{day}$). The authors then suggest a diffusion coefficient of the order of $10^6\ \mu\text{m}^2/\text{h} = 24\ \text{mm}^2/\text{day}$. However, they also used the same technique to determine the diffusion coefficient at the cell surface; this time the diffusion coefficient is estimated to be approximately $10^4\ \mu\text{m}^2/\text{h} = 0.24\ \text{mm}^2/\text{day}$. Keeping in mind all these considerations, for the model we take the intermediate value $D_V = 2.4\ \text{mm}^2/\text{day}$.

TGF-β Diffusion Coefficient D_T

In Lee et al. (2014) the authors estimate a TGF-β diffusion coefficient of $0.36\ \text{mm}^2/\text{h} = 8.64\ \text{mm}^2/\text{day}$ from Brown (1999), Goodhill (1997). In Murphy et al. (2012), the authors estimate a TGF-β diffusion coefficient of $2.54\ \text{mm}^2/\text{day}$ using the Stokes–Einstein Formula.

We checked their consistency with the estimate for D_V above. The Stokes–Einstein equation of these calculated values assumes spherical particles of radius r to have diffusion coefficient $D \sim 1/r$; since the molecular weight w of a particle is proportional to its volume, we have that $D \sim 1/\sqrt[3]{w}$ and thus $D_T \approx 2.76$.

Macrophage Random Motility μ_M

In Farrell et al. (1990), we find "Population random motility was characterised by the random motility coefficient, μ, which was mathematically equivalent to a diffusion coefficient. μ varied little over a range of C5a [a protein] concentrations with a minimum of $0.86 \times 10^{-8}\text{cm}^2/\text{sec}$ in 1×10^{-7} M C5a to a maximum of $1.9 \times 10^{-8}\text{cm}^2/\text{sec}$ in 1×10^{-11} M C5a". We thus take μ_M to be the average of these two values, that is $\mu_M = 1.38 \times 10^{-8}\text{cm}^2/\text{s} \approx 0.12\ \text{mm}^2/\text{day}$.

Advection Parameters λ_1 and λ_2

We will take λ_2^{chem} to be equal to v_{IF} calculated in "Appendix of Sizes, Weights, Equilibria and Velocities"; thus, $\lambda_2^{\text{chem}} = 864$ mm/day. For λ_1^{chem}, it is more complicated, but we would say that if C_{op} reaches the maximum possible value $C_{\max}$ calculated

in "Appendix of Maximum Capillary Density $C_{\max}$", then $\lambda_1^{\text{chem}} \cdot C_{\text{op}} = v_{\text{lymph}}$, which was calculated in "Appendix of Sizes, Weights, Equilibria and Velocities". That is, we assume that if the skin is "packed" with open capillaries, then the resulting flow will be the same as the usual lymph flow in the skin lymphatics). Hence, $\lambda_1^{\text{chem}} = v_{\text{lymph}}/C_{\max} = 0.0135$ mm day^{-1}cell^{-1}. For cells, we assume smaller values due the higher friction that cells encounter in the tissue. In the absence of relevant empirical data, we take $\lambda_1^{\text{cell}} = 1/10 \cdot \lambda_1^{\text{chem}}$ and $\lambda_2^{\text{cell}} = 1/10 \cdot \lambda_2^{\text{chem}}$.

Rate at Which TGF-β is Internalised by Macrophages γ_1

At equilibrium, $C = C^{\text{eq}}$ and thus $p(C) = 0$. Therefore, the equation for T at equilibrium becomes

$$a_M M^{\text{eq}}(T_L + r_1 M^{\text{eq}}) - d_1 T^{\text{eq}} - \gamma_1 T^{\text{eq}} M^{\text{eq}} = 0,$$

which leads to

$$\gamma_1 = \frac{a_M M^{\text{eq}}(T_L + r_1 M^{\text{eq}}) - d_1 T^{\text{eq}}}{T^{\text{eq}} M^{\text{eq}}} \approx 0.0042 \, \frac{\text{mm}^3}{\text{cells} \cdot \text{day}}.$$

Chemotaxis Parameters

Macrophage Chemotactic Sensitivity Towards TGF-β χ_1

In Li Jeon et al. (2002, Table 1), the chemotaxis coefficients of neutrophils for different gradients of interleukin-8 are listed (ranging from 0.6×10^{-7} to 12×10^{-7} mm^2·mL·ng^{-1}·s^{-1}). We take the intermediate value $\chi_1 = 5 \times 10^{-7}$mm^{2}mL ng^{-1}s^{-1} $\approx 4 \times 10^{-2}$mm^2(pg/mm^3)$^{-1}$day^{-1}. To compare this value with one from another source, we consider Tranquillo et al. (1988, Figure 8): although the chemotaxis coefficient is shown to depend on the attractant concentration, an average value is $\chi = 150$ cm^{2}sec^{-1}M^{-1} $\approx 5.18 \times 10^{-2}$mm^2(pg/mm^3)$^{-1}$day^{-1} (using the TGF-$\beta$ molecular weight found in "Appendix of TGF-β Molecular Weight and Equilibrium T^{eq}"). This result is encouraging because it is of the same order of magnitude as the previous estimate.

LEC Chemotactic Sensitivity Towards VEGF χ_2

In Barkefors et al. (2008), a quantification is made of the effects of FGF2 and VEGF165 on HUVEC and HUAEC chemotaxis. In Barkefors et al. (2008, Figure 6A), it is reported that the total distance migrated per HUVEC in response to a 50 ng/mL gradient of VEGFA165 was about 150 μm. Considering that the analysed area of the cell migration chamber was 800 μm long and that the experiment lasted 200 minutes, we can estimate the endothelial cell velocity to be 150/200 = 0.75 μm/min = 1.08 mm/day and the VEGF gradient to be 50 ng/mL / 800 μm = 62.50 (pg/mm^3)/mm. Now, the flux $\mathcal{J}$ in our equation is given by $\mathcal{J} = \chi_2 L \frac{\partial V}{\partial x}$; however, $\mathcal{J}$ can also be

seen as the product of the mass density and the velocity of the flowing mass (Douglas et al. 2005). Therefore, with L being our mass density, we have

$$\text{cell velocity} = \chi_2 \frac{\partial V}{\partial x}$$

and then we can use the previous calculations to estimate

$$\chi_2 = \frac{\text{cell velocity}}{\text{VEGF gradient}} = \frac{1.08\text{mm/day}}{62.50(\text{pg/mm}^3)/\text{mm}} = 0.0173 \frac{\text{mm}^2}{\text{day}} \frac{\text{mm}^3}{\text{pg}}.$$

In order to have realistic cell movement dynamics, χ_2 is taken to be 10 times bigger. This can be justified by the fact that the aforementioned data refer to HUVECs, and LECs might be faster than these cell types. A more suitable data set for this parameter would be very useful to better inform this estimate, but we are not aware of such data. Also, chemical gradients created *in vitro* are usually different between those observed *in vivo* and they are known to highly affect cell velocity.

Density Dependence of the Macrophage Chemotactic Sensitivity ω

The cell density dependence of the macrophage velocity is given by the factor $1/(1 + \omega M)$. This velocity is maximal when M is close to zero, and we assume that it is halved when M reaches its carrying capacity k_1^{old} (that is, the parameter k_1 in Bianchi et al. (2015)). We therefore take ω to be the inverse of the macrophage-carrying capacity k_1^{old}.

Macrophage Inflow ϕ_1

We expect ϕ_1 to be proportional to the lymph flow (estimated in "Appendix of Sizes, Weights, Equilibria and Velocities" as $v_{\text{lymph}} = 864\ \text{mm day}^{-1}$) and macrophage presence in the lymph. In the same source Fischer et al. (1996) that we used to estimate v_{lymph}, it is reported that the mean capillary diameter is 55 μm. Thus, about 2.05 mm^3 of lymph pass through a capillary bi-dimensional section in 1 day.

In Cao et al. (2005), we find that a mouse leucocyte count in the blood is approximately 3 to 8 $\times 10^6$ cells/mL and that of these about 2×10^6 are macrophages coming from the lymph nodes; so we have a macrophage density of 2×10^3 cells/mm^3 in the lymph. Therefore, each day about 2.05 mm^3 $\times$ 2×10^3 cells/mm^3 $= 4.11 \times 10^3$ macrophages pass in one capillary. Converting capillaries into cell density as was done in "Appendix of Maximum Capillary Density $C_{\max}$", we have an influx equal to $\frac{4.11}{20} \times 10^3 \text{day}^{-1} = 0.205 \times 10^3 \text{day}^{-1}$. However, the macrophage density reported in Cao et al. (2005) refers to blood; we assume that this quantity in lymph (especially during inflammation) will be about 10 times bigger. Therefore, we will take $\phi_1 = 2.05 \times 10^3 \text{day}^{-1}$.

References

Adams RH, Alitalo K (2007) Molecular regulation of angiogenesis and lymphangiogenesis. Nat Rev Mol Cell Biol 8(6):464–478

Ambrose CT (2006) Immunology's first priority dispute-an account of the 17th-century Rudbeck–Bartholin feud. Cell Immunol 242(1):1–8

Asai J, Takenaka H, Hirakawa S, Sakabe J, Hagura A, Kishimoto S, Maruyama K, Kajiya K, Kinoshita S, Tokura Y, Katoh N (2012) Topical simvastatin accelerates wound healing in diabetes by enhancing angiogenesis and lymphangiogenesis. Am J Pathol 181(6):2217–2224

Barkefors I, Le Jan S, Jakobsson L, Hejll E, Carlson G, Johansson H, Jarvius J, Park JW, Li Jeon N, Kreuger J (2008) Endothelial cell migration in stable gradients of vascular endothelial growth factor A and fibroblast growth factor 2: effects on chemotaxis and chemokinesis. J Biol Chem 283(20):13905–13912

Benest AV, Harper SJ, Herttuala SY, Alitalo K, Bates DO (2008) VEGF-C induced angiogenesis preferentially occurs at a distance from lymphangiogenesis. Cardiovasc Res 78(2):315–323

Bernatchez PN, Soker S, Sirois MG (1999) Vascular endothelial growth factor effect on endothelial cell proliferation, migration, and platelet-activating factor synthesis is Flk-1-dependent. J Biol Chem 274(43):31047–31054

Bianchi A, Painter KJ, Sherratt JA (2015) A mathematical model for lymphangiogenesis in normal and diabetic wounds. J Theor Biol 383:61–86

Boardman KC, Swartz MA (2003) Interstitial flow as a guide for lymphangiogenesis. Circ Res 92:801–808

Boulton R, Woodman A, Calnan D, Selden C, Tam F, Hodgson H (1997) Nonparenchymal cells from regenerating rat liver generate interleukin-1alpha and -1beta: a mechanism of negative regulation of hepatocyte proliferation. Hepatology 26(1):49–58

Brem H, Tomic-Canic M (2007) Cellular and molecular basis of wound healing in diabetes. J Clin Invest 117(5):1219–1222

Brown DR (1999) Dependence of neurones on astrocytes in a coculture system renders neurones sensitive to transforming growth factor β1-induced glutamate toxicity. J Neurochem 72(3):943–953

Byrne HM, Chaplain MAJ (1995) Explicit solutions of a simplified model of capillary sprout growth during tumour angiogenesis. Appl Math Lett 8(5):71–76

Byrne HM, Chaplain MAJ, Evans DL, Hopkinson I (2000) Mathematical modelling of angiogenesis in wound healing: comparison of theory and experiment. J Theor Med 2(3):175–197

Cao C, Lawrence DA, Strickland DK, Zhang L (2005) A specific role of integrin Mac-1 in accelerated macrophage efflux to the lymphatics. Blood 106(9):3234–3241

Cao Y (2005) Opinion: emerging mechanisms of tumour lymphangiogenesis and lymphatic metastasis. Nat Rev Cancer 5(9):735–743

Castiglioni A (1947) A history of medicine. Alfred A. Knopf, New York

Chaplain MAJ, Anderson ARA (1999) Modelling the growth and form of capillary networks. In: On growth and form: spatio-temporal pattern formation in biology, Wiley, pp 225–250

Chaplain MAJ, McDougall SR, Anderson ARA (2006) Mathematical modeling of tumor-induced angiogenesis. Annu Rev Biomed Eng 8:233–257

Cho CH, Sung HK, Kim KT, Cheon HG, Oh GT, Hong HJ, Yoo OJ, Koh GY (2006) COMP-angiopoietin-1 promotes wound healing through enhanced angiogenesis, lymphangiogenesis, and blood flow in a diabetic mouse model. PNAS 103(13):4946–4951

Choi I, Lee S, Hong YK (2012) The new era of the lymphatic system: no longer secondary to the blood vascular system. Cold Spring Harb Perspect Med 2(4):a006,445

Christiansen A, Detmar M (2011) Lymphangiogenesis and cancer. Genes Cancer 2(12):1146–1158

Cobbold CA, Sherratt JA (2000) Mathematical modelling of nitric oxide activity in wound healing can explain keloid and hypertrophic scarring. J Theor Biol 204:257–288

De Crescenzo G, Grothe S, Zwaagstra J, Tsang M, O'Connor-McCourt MD (2001) Real-time monitoring of the interactions of transforming growth factor-β (TGF-β) isoforms with latency-associated protein and the ectodomains of the TGF-β type II and III receptors reveals different kinetic models and stoichiometries of binding. J Biol Chem 276(32):29632–29643

Dodson JF (1924-1925) Herophilus of alexandria. Proc R Soc Med 18:19–32

Douglas JF, Gasiorek JM, Swaffield JA, Jack LB (2005) Fluid mechanics, 5th edn. Prentice Hall, Upper Saddle River

Drew P, Posnett J, Rusling L (2007) The cost of wound care for a local population in England. Int Wound J 4(2):149–155

Edelstein L (1982) The propagation of fungal colonies: a model for tissue growth. J Theor Biol 98:679–701

Farrell BE, Daniele RP, Lauffenburger DA (1990) Quantitative relationships between single-cell and cell-population model parameters for chemosensory migration responses of alveolar macrophages to C5a. Cell Motil Cytoskelet 16(4):279–293

Fischer M, Costanzo U, Hoffmann U, Bollinger A, Franzeck UK (1997) Flow velocity of cutaneous lymphatic capillaries in patients with primary lymphedema. Int J Microcirc Clin Exp 17(3):143–149

Fischer M, Franzeck UK, Herrig I, Costanzo U, Wen S, Schiesser M, Hoffmann U, Bollinger A (1996) Flow velocity of single lymphatic capillaries in human skin. Am J Physiol 270(1 Pt 2):H358–H363

Flegg JA, Byrne HM, Flegg MB, McElwain DLS (2012) Wound healing angiogenesis: the clinical implications of a simple mathematical model. J Theor Biol 300:309–316

Flegg JA, Menon SN, Maini PK, McElwain DLS (2015) On the mathematical modeling of wound healing angiogenesis in skin as a reaction-transport process. Front Physiol 6:262. doi:10.3389/fphys.2015.00262

Fleury ME, Boardman KC, Swartz MA (2006) Autologous morphogen gradients by subtle interstitial flow and matrix interactions. Biophys J 91:113–121

Friedman A, Lolas G (2005) Analysis of a mathematical model of tumor lymphangiogenesis. Math Models Methods Appl Sci 15(1):95–107

Galie P, Spilker RL (2009) A two-dimensional computational model of lymph transport across primary lymphatic valves. J Biomech Eng 131(11):111,004

Goldman J, Rutkowski JM, Shields JD, Pasquier MC, Cui Y, Schmokel HG, Willey S, Hicklin DJ, Pytowski B, Swartz MA (2007) Cooperative and redundant roles of VEGFR-2 and VEGFR-3 signaling in adult lymphangiogenesis. FASEB J 21(4):1003–1012

Goodhill GJ (1997) Diffusion in axon guidance. Eur J Neurosci 9(7):1414–1421

Gosiewska A, Yi C, Blanc-Brude O, Geesin JC (1999) Characterization of a macrophage-based system for studying the activation of latent TGF-β. Methods Cell Sci 21:47–56

Grainger DJ, Wakefield L, Bethell HW, Farndale RW, Metcalfe JC (1995) Release and activation of platelet latent TGF-beta in blood clots during dissolution with plasmin. Nat Med 1(9):932–937

Greenwood B (1973) The mitosis of sheep blood monocytes in tissue culture. Q J Exp Physiol 58:369–377

Haas TL, Duling BR (1997) Morphology favors an endothelial cell pathway for longitudinal conduction within arterioles. Microvasc Res 53:113–120

Helm CL, Fleury ME, Zisch AH, Boschetti F, Swartz MA (2005) Synergy between interstitial flow and VEGF directs capillary morphogenesis in vitro through a gradient amplification mechanism. Proc Natl Acad Sci USA 102(44):15779–15784

Heppell C, Roose T, Richardson G (2015) A model for interstitial drainage through a sliding lymphatic valve. Bull Math Biol 77:1101–1131

Hormbrey E, Han C, Roberts A, McGrouther DA, Harris AL (2003) The relationship of human wound vascular endothelial growth factor (VEGF) after breast cancer surgery to circulating vegf and angiogenesis. Clin Cancer Res 9:4332–4339

Huggenberger R, Siddiqui SS, Brander D, Ullmann S, Zimmermann K, Antsiferova M, Werner S, Alitalo K, Detmar M (2011) An important role of lymphatic vessel activation in limiting acute inflammation. Blood 117(17):4667–4678

Hyytiäinen M, Penttinen C, Keski-Oja J (2004) Latent TGF-beta binding proteins: extracellular matrix association and roles in TGF-beta activation. Crit Rev Clin Lab Sci 41(3):233–264

Jeffcoate WJ, Harding KG (2003) Diabetic foot ulcers. Lancet 361(9368):1545–1551

Ji RC (2005) Characteristics of lymphatic endothelial cells in physiological and pathological conditions. Histol Histopathol 20:155–175

Kaminska B, Wesolowska A, Danilkiewicz M (2005) TGF beta signalling and its role in tumor pathogenesis. Acta Biochim Pol 52(2):329–337

Kaur H, Yung LY (2012) Probing high affinity sequences of DNA aptamer against VEGF165. PLoS ONE 7(2):e31,196

Khalil N, Corne S, Whitman C, Yacyshyn H (1996) Plasmin regulates the activation of cell-associated latent TGF-beta 1 secreted by rat alveolar macrophages after in vivo bleomycin injury. Am J Respir Cell Mol Biol 15(2):252–259

Khalil N, Whitman C, Zuo L, Danielpour D, Greenberg A (1993) Regulation of alveolar macrophage transforming growth factor-β secretion by corticosteroids in bleomycin-induced pulmonary inflammation in the rat. J Clin Invest 92:1812–1818

Kiriakidis S, Andreakos E, Monaco C, Foxwell B, Feldmann M, Paleolog E (2003) VEGF expression in human macrophages is NF-κB-dependent: studies using adenoviruses expressing the endogenous NF-κB inhibitor IκBα and a kinase-defective form of the IκB kinase 2. J Cell Sci 116(4):665–674

Kleinheinz J, Jung S, Wermker K, Fischer C, Joos U (2010) Release kinetics of $VEGF_{165}$ from a collagen matrix and structural matrix changes in a circulation model. Head Face Med 6:17. doi:10.1186/1746-160X-6-17

Krombach F, Munzing S, Allmeling AM, Gerlach JT, Behr J, Dorger M (1997) Cell size of alveolar macrophages: an interspecies comparison. Environ Health Perspect 105(Suppl 5):1261–1263

Lee S, Hwang HJ, Kim Y (2014) Modeling the role of TGF-β in regulation of the Th17 phenotype in the LPS-driven immune system. Bull Math Biol 76(5):1045–1080

Levine HA, Pamuk S, Sleeman BD, Nilsen-Hamilton M (2001) Mathematical modeling of capillary formation and development in tumor angiogenesis: penetration into the stroma. Bull Math Biol 63(5):801–863

Li Jeon N, Baskaran H, Dertinger SK, Whitesides GM, Van de Water L, Toner M (2002) Neutrophil chemotaxis in linear and complex gradients of interleukin-8 formed in a microfabricated device. Nat Biotechnol 20(8):826–830

Lohela M, Bry M, Tammela T, Alitalo K (2009) VEGFs and receptors involved in angiogenesis versus lymphangiogenesis. Curr Opin Cell Biol 21(2):154–165

Louveau A, Smirnov I, Keyes TJ, Eccles JD, Rouhani SJ, Peske JD, Derecki NC, Castle D, Mandell JW, Lee KS, Harris TH, Kipnis J (2015) Structural and functional features of central nervous system lymphatic vessels. Nature 523(7560):337–341

Ludwig D, Aronson DG, Weinberger HF (1979) Spatial patterning of the spruce budworm. J Math Biol 8:217–258

Lunt SJ, Kalliomaki TM, Brown A, Yang VX, Milosevic M, Hill RP (2008) Interstitial fluid pressure, vascularity and metastasis in ectopic, orthotopic and spontaneous tumours. BMC Cancer 8:2

Mac Gabhann F, Popel AS (2004) Model of competitive binding of vascular endothelial growth factor and placental growth factor to VEGF receptors on endothelial cells. Am J Physiol Heart Circ Physiol 286:H153–H164

Macdonald AJ, Arkill KP, Tabor GR, McHale NG, Winlove CP (2008) Modeling flow in collecting lymphatic vessels: one-dimensional flow through a series of contractile elements. Am J Physiol Heart Circ Physiol 295(1):H305–313

Mantovani A, Sica A, Sozzani S, Allavena P, Vecchi A, Locati M (2004) The chemokine system in diverse forms of macrophage activation and polarization. Trends Immunol 25(12):677–686

Mantzaris NV, Webb S, Othmer HG (2004) Mathematical modeling of tumor-induced angiogenesis. J Math Biol 49:111–187

Margaris KN, Black RA (2012) Modelling the lymphatic system: challenges and opportunities. J R Soc Interface 9(69):601–612

Maruyama K, Asai J, Ii M, Thorne T, Losordo DW, D'Amore PA (2007) Decreased macrophage number and activation lead to reduced lymphatic vessel formation and contribute to impaired diabetic wound healing. Am J Pathol 70:1178–1191

May MTGT (1968) Galen on the usefulness of the parts of the body. Part II. Cornell University Press, Ithaca

Mendoza E, Schmid-Schönbein GW (2003) A model for mechanics of primary lymphatic valves. J Biomech Eng 125:407–414

Miura T, Tanaka R (2009) In vitro vasculogenesis models revisited—measurement of VEGF diffusion in matrigel. Math Model Nat Phenom 4(4):118–130

Monstrey S, Hoeksema H, Verbelen J, Pirayesh A, Blondeel P (2008) Assessment of burn depth and burn wound healing potential. Burns 34:761–769

Müller G, Behrens J, Nussbaumer U, Böhlen P, Birchmeier W (1987) Inhibitory action of transforming growth factor β on endothelial cells. PNAS 84:5600–5604

Murphy KE, Hall CL, Maini PK, McCue SW, McElwain DLS (2012) A fibrocontractive mechanochemical model of dermal wound closure incorporating realistic growth factor kinetics. Bull Math Biol 74(5):1143–1170

Nguyen VPKH, Chen SH, Trinh J, Kim H, Coomber BL, Dumont DJ (2007) Differential response of lymphatic, venous and arterial endothelial cells to angiopoietin-1 and angiopoietin-2. BMC Cell Biol 8:10

Norrmen C, Tammela T, Petrova TV, Alitalo K (2011) Biological basis of therapeutic lymphangiogenesis. Circulation 123(12):1335–1351

Nunes I, Shapiro RL, Rifkin DB (1995) Characterization of latent TGF-β activation by murine peritoneal macrophages. J Immunol 155:1450–1459

Oi M, Yamamoto T, Nishioka K (2004) Increased expression of TGF-β1 in the sclerotic skin in bleomycin-'susceptible' mouse strains. J Med Dent Sci 51:7–17

Oliver G, Detmar M (2002) The rediscovery of the lymphatic system: old and new insights into the development and biological function of the lymphatic vasculature. Genes Dev 16(7):773–783

Papaioannou AI, Zakynthinos E, Kostikas K, Kiropoulos T, Koutsokera A, Ziogas A, Koutroumpas A, Sakkas L, Gourgoulianis KI, Daniil ZD (2009) Serum VEGF levels are related to the presence of pulmonary arterial hypertension in systemic sclerosis. BMC Pulm Med 9:18

Pierce GF (2001) Inflammation in nonhealing diabetic wounds: the space–time continuum does matter. Am J Pathol 159(2):399–403

Podgrabinska S, Braun P, Velasco P, Kloos B, Pepper MS, Jackson D, Skobe M (2002) Molecular characterization of lymphatic endothelial cells. PNAS 99(25):16069–16074

Posnett J, Franks PJ (2008) The burden of chronic wounds in the UK. Nurs Times 104(3):44–45

Reddy NP, Patel K (1995) A mathematical model of flow through the terminal lymphatics. Med Eng Phys 17(2):134–140

Rofstad EK, Galappathi K, Mathiesen BS (2014) Tumor interstitial fluid pressure—a link between tumor hypoxia, microvascular density, and lymph node metastasis. Neoplasia 16(7):586–594

Roose T, Fowler AC (2008) Network development in biological gels: role in lymphatic vessel development. Bull Math Biol 70(6):1772–1789

Rutkowski JM, Boardman KC, Swartz MA (2006) Characterization of lymphangiogenesis in a model of adult skin regeneration. Am J Physiol Heart Circ Physiol 291:H1402–H1410

Rutkowski JM, Swartz MA (2007) A driving force for change: interstitial flow as a morphoregulator. Trends Cell Biol 17(1):44–50

Saaristo A, Tammela T, Farkkila A, Karkkainen M, Suominen E, Yla-Herttuala S, Alitalo K (2006) Vascular endothelial growth factor-C accelerates diabetic wound healing. Am J Pathol 169:1080–1087

Schugart RC, Friedman A, Zhao R, Sen CK (2008) Wound angiogenesis as a function of tissue oxygen tension: a mathematical model. PNAS 105(7):2628–2633

Scianna M, Bell CG, Preziosi L (2013) A review of mathematical models for the formation of vascular networks. J Theor Biol 333:174–209

Sheikh AY, Gibson JJ, Rollins MD, Hopf HW, Hussain Z, Hunt TK (2000) Effect of hyperoxia on vascular endothelial growth factor levels in wound model. Arch Surg 135:1293–1297

Shi M, Zhu J, Wang R, Chen X, Mi L, Walz T, Springer TA (2011) Latent TGF-β structure and activation. Nature 474:343–351

Shields JD, Fleury ME, Yong C, Tomei AA, Randolph GJ, Swartz MA (2007) Autologous chemotaxis as a mechanism of tumor cell homing to lymphatics via interstitial flow and autocrine ccr7 signaling. Cancer Cell 11(6):526–538

Simonsen TG, Gaustad JV, Leinaas MN, Rofstad EK (2012) High interstitial fluid pressure is associated with tumor-line specific vascular abnormalities in human melanoma xenografts. PLoS ONE 7(6):e40,006

Singer AJ, Clark RA (1999) Cutaneous wound healing. N Engl J Med 341(10):738–746

Stadelmann WK, Digenis AG, Tobin GR (1998) Physiology and healing dynamics of chronic cutaneous wounds. Am J Surg 176(2A Suppl):26S–38S

Stéphanou A, McDougall SR, Anderson ARA, Chaplain MAJ (2005) Mathematical modelling of flow in 2D and 3D vascular networks: applications to anti-angiogenic and chemotherapeutic drug strategies. Math Comput Model 41(10):1137–1156

Sutton AB, Canfield AE, Schor SL, Grant ME, Schor AM (1991) The response of endothelial cells to TGFβ-1 is dependent upon cell shape, proliferative state and the nature of the substratum. J Cell Sci 99:777–787

Sweat RS, Stapor PC, Murfee WL (2012) Relationships between lymphangiogenesis and angiogenesis during inflammation in rat mesentery microvascular networks. Lymphat Res Biol 10(4):198–207

Swift ME, Burns AL, Gray KL, DiPietro LA (2001) Age-related alterations in the inflammatory response to dermal injury. J Invest Dermatol 117(5):1027–1035

Tammela T, Alitalo K (2010) Lymphangiogenesis: molecular mechanisms and future promise. Cell 140:460–476

Taylor AW (2009) Review of the activation of TGF-β in immunity. J Leukoc Biol 85:29–33

Tranquillo RT, Zigmond SH, Lauffenburger DA (1988) Measurement of the chemotaxis coefficient for human neutrophils in the under-agarose migration assay. Cell Motil Cytoskelet 11(1):1–15

van den Berg BM, Vink H, Spaan JAE (2003) The endothelial glycocalyx protects against myocardial edema. Circ Res 92:592–594

Velázquez JJL (2004a) Point dynamics in a singular limit of the Keller–Segel model 1: motion of the concentration regions. SIAM J Appl Math 64(4):1198–1223

Velázquez JJL (2004b) Point dynamics in a singular limit of the Keller–Segel model 2: formation of the concentration regions. SIAM J Appl Math 64(4):1224–1248

von Staden H (1989) Herophilus [and] the art of medicine in early alexandria. Cambridge University Press, Cambridge

Vowden P (2011) Hard-to-heal wounds Made Easy. Wounds Int 2(4). http://www.woundsinternational.com

Wahl SM, Hunt DA, Wakefield LM, McCartney-Francis N, Wahl LM, Roberts AB, Sporn MB (1987) Transforming growth factor type β induces monocyte chemotaxis and growth factor production. PNAS 84:5788–5792

Wakefield LM, Smith DM, Flanders KC, Sporn MB (1988) Latent transforming growth factor-beta from human platelets. A high molecular weight complex containing precursor sequences. J Biol Chem 263(16):7646–7654

Waugh HV, Sherratt JA (2006) Macrophage dynamics in diabetic wound healing. Bull Math Biol 68:197–207

Weber-Matthiesen K, Sterry W (1990) Organization of the monocyte/macrophage system of normal human skin. J Invest Dermatol 95:83–89

Whitehurst B, Eversgerd C, Flister M, Bivens CM, Pickett B, Zawieja DC, Ran S (2006) Molecular profile and proliferative responses of rat lymphatic endothelial cells in culture. Lymph Res Biol 4(3):119–142

Withington ETT (1984) Hippocrates on joints, vol 3. Harvard University Press, Cambridge

Witte MH, Bernas MJ, Martin CP, Witte CL (2001) Lymphangiogenesis and lymphangiodysplasia: from molecular to clinical lymphology. Microsc Res Tech 55:122–145

Yang JP, Liu HJ, Cheng SM, Wang ZL, Cheng X, Yu HX, Liu XF (2009) Direct transport of VEGF from the nasal cavity to brain. Neurosci Lett 449(2):108–111

Yang L, Qiu CX, Ludlow A, Ferguson MWJ, Brunner G (1999) Active transforming growth factor-β in wound repair—determination using a new assay. Am J Pathol 154(1):105–111

Zachary I, Gliki G (2001) Signaling transduction mechanisms mediating biological actions of the vascular endothelial growth factor family. Cardiovasc Res 49:568–581

Zheng Y, Watanabe M, Kuraishi T, Hattori S, Kai C, Shibuya M (2007) Chimeric VEGF-ENZ7/PlGF specifically binding to VEGFR-2 accelerates skin wound healing via enhancement of neovascularization. Arterioscler Thromb Vasc Biol 27(3):503–511

Zhuang JC, Wogan GN (1997) Growth and viability of macrophages continuously stimulated to produce nitric oxide. PNAS 94:11875–11880

Zimny S, Schatz H, Pfohl M (2002) Determinants and estimation of healing times in diabetic foot ulcers. J Diabetes Complic 16(5):327–332